

JGR Earth Surface

RESEARCH ARTICLE

10.1029/2022JF006712

Key Points:

- Field observation data of 93 debrisflow events at Jiangjia Ravine (Yunnan Province, China) are systematically analyzed
- The flow resistance of the Jiangjia Ravine debris flows can be unified by a visco-collisional scaling law
- Manning's formula is modified by the visco-collisional scaling law, which gives Manning's coefficient an explicit physical meaning

Correspondence to:

D. Song, drsong@imde.ac.cn

Citation:

Chen, Q., Song, D., Chen, X., & Zhong, W. (2023). Visco-collisional scaling law of flow resistance and its application in debris-flow mobility. *Journal of Geophysical Research: Earth Surface*, 128, e2022JF006712. https://doi.org/10.1029/2022JF006712

Received 15 APR 2022 Accepted 12 JAN 2023

Author Contributions:

Conceptualization: Qian Chen,
Dongri Song
Data curation: Wei Zhong
Formal analysis: Qian Chen, Dongri Song
Funding acquisition: Dongri Song,
Xiaoqing Chen

Methodology: Qian Chen, Dongri Song Project Administration: Xiaoqing Chen Supervision: Dongri Song, Xiaoqing Chen Validation: Qian Chen, Wei Zhong Writing – original draft: Qian Chen Writing – review & editing: Qian Chen, Wei Zhong

Visco-Collisional Scaling Law of Flow Resistance and Its Application in Debris-Flow Mobility

Qian Chen^{1,2}, Dongri Song^{1,2}, Xiaoqing Chen^{1,2}, and Wei Zhong^{1,2}

¹Institute of Mountain Hazards and Environment, Chinese Academy of Sciences, Chengdu, China, ²University of Chinese Academy of Sciences, Beijing, China

Abstract Flow resistance against gravity-driven forces is a key factor controlling debris-flow mobility, which is an important parameter for hazard risk assessment. In practice, Manning's formula is widely used for debris-flow mobility analysis. However, this formula depends on the boundary conditions (channel roughness) and neglects the physical mechanisms of debris flow. Based on the systematic analysis of the field observation data of 93 debris-flow events at Jiangjia Ravine (Yunnan Province, China), this study investigates the dynamic mechanisms and sources of flow resistance of debris flow. As the flows tend to be liquefied, the fluid viscous effect and particle collisions are the main sources of flow resistance. Flow resistance can be described by a visco-collisional scaling law. Under fixed channel boundary conditions, this law is further incorporated into Manning's formula, bridging the gap between the resistance model based on physical mechanisms and the empirical formula of flow resistance. The modified Manning's coefficient is closely related to flow regimes, giving Manning's coefficient an explicit physical meaning. The modified Manning's coefficient provides a more reasonable basis for the mobility analysis and risk assessment of debris flow.

Plain Language Summary Debris flows are the common geological hazards composed of solid particles and fluids. Debris flows with different volumetric solid concentrations result in distinct mobility. Flow resistance is a key factor controlling mobility, and the flow resistance of debris flow mainly comes from the contribution of solid and fluid phases. However, in practical applications, the flow resistance is estimated using empirical formulas that do not consider the solid-fluid interaction. To provide a more reasonable basis for debris-flow risk assessment, this study systematically analyzes the field observation data of 93 debris-flow events in Jiangjia Ravine (Yunnan Province, China), explores the physical mechanisms of the movement of natural debris flows and reveals the source of flow resistance. A physical model that reflects the resistance characteristics of natural debris flows is proposed. Furthermore, the resistance model is substituted into the empirical formula. The modified empirical formula (Manning's formula) has a clear physical meaning and is helpful for debris-flow risk assessment.

1. Introduction

For geophysical flows, such as debris flows and lahars, flow resistance against gravity-driven forces is the key to flow mobility analysis. The accurate quantification of flow resistance provides a basis for catchment-scale hazard risk assessment as well as key parameters for engineering mitigation. Based on energy conservation in a steady flow, the mechanical energy required to overcome the flow resistance is equal to the head loss along the path. For steady flow, the expression of flow resistance is

$$\tau = \rho g h S \tag{1}$$

where τ is the shear stress (Pa), ρ is the bulk density of flow (kg/m³), h is the flow depth (m), g is the acceleration of gravity (9.81 m/s²), $S = \sin \theta$, and θ is the channel inclination (°).

External and internal factors jointly affect the flow resistance of debris flow. The former includes the roughness and geometry of the channel, and accordingly, the resulting flow resistance is the result of the interaction between the channel boundary (bed and sidewall) and debris flow (Nikora et al., 1998; Rickenmann, 1999; Stewart et al., 2019). The latter is related to the material composition and flow regime of the debris flow. The resulting flow resistance comes from the fluid viscous effect and solid particle interactions, which finally transfer to the interface between the debris flow and boundary (Ancey, 2007; Bagnold, 1954; Iverson, 1997). Accordingly, the research methods can be categorized into empirical approaches and physical models. The former originates from

© 2023. American Geophysical Union. All Rights Reserved.

CHEN ET AL. 1 of 22



the open channel flow in hydraulics, where the roughness coefficients are used to quantify the flow resistance of geophysical flows (Huybrechts et al., 2011; Julien & Paris, 2010; Rickenmann, 1999). The latter focuses on the contribution of internal stresses (solid-fluid interaction) to the flow resistance (Bagnold, 1954; Boyer et al., 2011; Du et al., 2021; Iverson, 1997; Trulsson et al., 2012).

The empirical approach for characterizing flow resistance by boundary roughness adopts equations widely used in hydraulics, including Chézy's formula and Manning's formula (Özgen et al., 2015; Stewart et al., 2019; Yen, 1992). In practice, Manning's formula is widely used for flash floods and debris flows because of its simple form and limited input parameters (Julien & Paris, 2010; Rickenmann, 1999; Yen, 1992). The expression of Manning's formula is

$$v = -\frac{1}{n}h^{2/3}S^{1/2} \tag{2}$$

where v is the velocity (m/s) and n is Manning's coefficient (m^{-1/3}s). Based on Manning's formula calibrated by field observation data, many improved equations for calculating debris-flow velocity have been proposed, and their applicability has been compared (Julien & Paris, 2010). In these modified empirical equations, Manning's coefficient is a function of channel roughness, flow depth, channel slope, and characteristic particle (Ferguson, 2005; Rickenmann, 1999) size. In addition, the shape of protrusion and vegetation at the channel bottom are also considered (Huthoff, 2012; Stewart et al., 2019).

Although the empirical approach characterized by roughness coefficients is widely used in sediment transport and debris flow, most of them are empirical equations (Chézy's formula and Manning's formula) modified by the field observation data of specific valleys. These empirical equations do not consider the mechanisms of geophysical flows, resulting in roughness coefficients that are highly empirical and site specific. In numerical simulations, Manning's coefficient is artificially set as a constant to back-calculate documented debris-flow events as well as to predict the consequences of potential hazard scenarios (Delaney & Evans, 2015; Sairam et al., 2021; Turzewski et al., 2019). In general, Manning's coefficient is a comprehensive coefficient of various factors that characterizes the boundary condition influencing the flow resistance without clear physical meaning (Cui et al., 2016).

The physical models of flow resistance can be traced back to the pioneering work of Hans A. Einstein in the early twentieth century. Adding particles to Newtonian fluids increases their viscosity and the relationship between effective viscosity and solid concentration is quantified (Einstein, 1905). In the case of neutrally buoyant particles under steady shear, the linearity of the Stokes equation implies that shear stress τ and shear rate $\dot{\gamma}$ are linearly related, that is, $\tau = \eta_s(\varphi_s)\eta\dot{\gamma}$, where η is the viscosity of Newtonian fluid (Pa·s) and η_s is the shear relative viscosity. The relative viscosity η_s increases with increasing solid concentration φ_s and diverges at the jamming transition where the solid concentration reaches its maximum φ_m (Stickel & Powell, 2005; Wildemuth & Williams, 1984). The above description of flow resistance is derived from the traditional fluid rheology framework, where the geophysical flows are equivalent to single-phase fluids and the shear stress (resistance) depends on the shear rate.

With further study on geophysical flows, researchers have found that the two-phase flow models that consider the interaction between particles (collision and friction (Bartelt et al., 2012; Iverson, 1997)) and the fluid viscous effect are potent in explaining the characteristics of geophysical flows. In dense two-phase flows, the feedback between the effective stress and pore fluid pressure caused by particle dilation plays a significant role in the movement of debris flow (Iverson, 2000, 2005; Pailha & Pouliquen, 2009), and a resistance model linking the microscopic solid-fluid interaction and the macroscopic dilation behavior is proposed (Iverson & George, 2014). Therefore, the contact friction provided by the effective stress is the main source of flow resistance, which shows longer coherence lengths (Lanzoni et al., 2017). The flows dominated by particle collisions are termed Bagnoldian flows, in which the shear stress is proportional to the square of the shear rate (Bagnold, 1954), and the constant coherence length value is 1–2 particle diameters (Lanzoni et al., 2017). The dependence of flow resistance τ on the particle normal stress σ promotes the macroscopic friction coefficient $\mu = \tau/\sigma$, which is a breakthrough for exploring the rheological relationship. The rheological relationship of dense two-phase flows is unified within the framework where the macroscopic friction coefficient μ is related to the time scale of particle interaction and viscous time scale, such as the $\mu(J)$ law (Boyer et al., 2011) and $\mu(K)$ law (Trulsson et al., 2012).

To reveal the flow mechanism, physical models of flow resistance mostly come from specific physical experiments (Bagnold, 1954; Boyer et al., 2011) or numerical simulations (Trulsson et al., 2012). Focusing on flows composed of specific particles and fluids, most physical models have not been applied to well-graded geophysical

CHEN ET AL. 2 of 22



flows in natural settings. In addition, existing physical models are mainly suitable for dense two-phase flows with nontrivial effective stress, rather than dilute cases without effective stress.

These resistance models are often embedded in depth-averaged equations to simulate the movement of debris flow, and their performances have been compared (Hungr & McDougall, 2009; Major et al., 2005; McDougall & Hungr, 2004; Naef et al., 2006; O'Brien et al., 1993). At present, there is no universal resistance model available to represent the flow resistance of debris flow. Debris flow is considered a quasi-homogeneous fluid, and the flow resistance is quantified by single-phase flow models. For example, the turbulent flow model is characterized by Manning's coefficient, the Bingham model depends on the fluid viscosity, the viscoplastic model considers the yield stress, and the friction-dominated Coulomb model. Alternatively, to reveal the contribution of solid and fluid phases to the flow resistance, the quantification of flow resistance is a combination of multiple submodels. In depth-averaged two-phase flow models, in order to close the governing equations, the conventional and effective practice is to divide the total basal resistance into the respective resistances imposed on the solid and fluid phases (Berzi & Larcan, 2013; Egashira, 2011; Iverson, 1997). The solid phase resistances are often assumed to satisfy the Coulomb friction law (J. Li et al., 2018; Ouyang et al., 2013), and the resistances of fluids are treated as non-Newtonian viscous stresses (Pudasaini, 2012; Pudasaini & Mergili, 2019) or estimated from empirical formulas with roughness coefficients, such as Manning's coefficient (Cao et al., 2015; Delaney & Evans, 2015; Sairam et al., 2021). These approaches of dealing with flow resistance appear to capture the movement of debris flow in depth-averaged equations; however, they do not bridge the gaps between current empirical approaches and physical models of flow resistance and the movement of natural debris flows.

In view of the above gaps in the empirical approach and physical models of flow resistance, this study systematically analyzes the field observation data of 93 debris-flow events at Jiangjia Ravine (Yunnan Province, China) and investigates the source of debris-flow resistance for cases with negligible effective stress. In this study, the 93 debris-flow events are divided into two groups to explore the influence of solid-fluid interactions on flow resistance. Based on a set of 34 debris-flow events from 1999 to 2001, a visco-collisional scaling law of flow resistance is established. Another set of 59 debris-flow events from 2002 to 2017 is used to verify this law. Manning's coefficient is further modified by this physical model, denoting an explicit physical meaning.

2. Field Observation of Debris Flow at Jiangjia Ravine

2.1. The Jiangjia Ravine

Jiangjia Ravine is located in Yunnan Province, China. It is a tributary of the Xiaojiang River in the upper reaches of the Yangtze River. As shown in Figure 1a, the specific geographical location is between N26°13′–N26°17′ and E103°06′–E103°13′. The main channel is 13.9 km long with a drainage area of 48.6 km² and extends from the drainage divide at 3,269 m altitude west to the junction with the Xiaojiang River at 1,042 m (Cui et al., 2005).

The bed rocks of the Jiangjia Ravine are Proterozoic shallow metamorphic slate and phyllite, which are poor in strength and easy to weather. Slate and phyllite are widely distributed upstream of the channel and are strongly affected by the tectonic activity. As a result, there are substantial number of loose materials stored in these valleys, up to 12.3 × 10⁹ m³ (Cui et al., 2005). The annual rainfall at Jiangjia Ravine varies from 700 to 1,200 mm, showing significant seasonality and vertical zonality. Approximately 85% of the total annual rainfall is concentrated from May to October, and approximately 40% of the rainfall occurs between altitudes of 2,500 and 3,000 m (Cui et al., 2005; Guo et al., 2020). Abundant loose materials and concentrated rainfall have created favorable conditions for the occurrence of debris flow. Under heavy rainfall, the debris in the valleys is eroded and entrained, forming debris flows (Cui et al., 2005; Zhou & Ng, 2010). Jiangjia Ravine is known for its high frequency of debris flow. On average, dozens of debris-flow events occur every year (28 events in 1965), and each event contains tens to hundreds of surges (Kang et al., 2004). Therefore, Jiangjia Ravine has become an ideal place for a debris-flow observation and is known as the "Debris flow Museum" in China (Davies, 1990).

In the 1960s, the Institute of Mountain Hazards and Environment, Chinese Academy of Sciences established the Dongchuan Debris Flow Observation and Research Station (DDFORS) at Jiangjia Ravine. Since the establishment of DDFORS, long-term observations and research on the initiation, transportation, and accumulation of debris flow have been carried out, and a relatively complete debris-flow database has been established, which contains more than 400 debris-flow events (Cui et al., 2005; Kang et al., 2004).

CHEN ET AL. 3 of 22

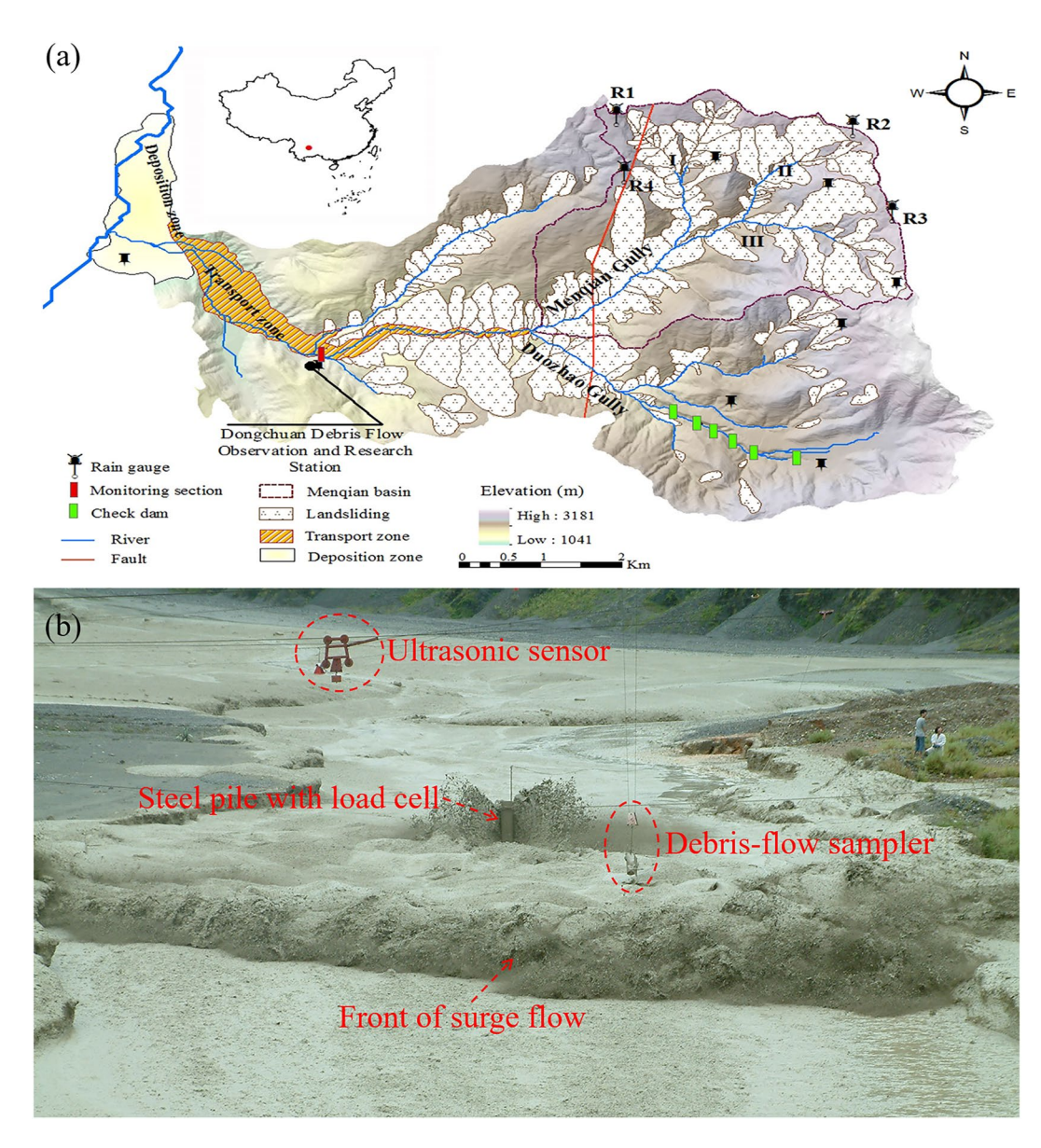


Figure 1. Jiangjia Ravine: (a) plan view (Guo et al., 2020) and (b) observation of debris flow at Dongchuan Debris Flow Observation and Research Station.

2.2. Debris Flow Observation at DDFORS

In DDFORS, the observation focuses on the kinetic parameters of debris flow. The measured physical quantities include the frontal velocity v (m/s), flow surface width W (m), flow depth h (m), and bulk density ρ (kg/m³). The specific measurement methods for these parameters are described as follows.

Before a debris flow occurs, a straight channel with a length of L is selected and marked to measure the debris flow velocity. Time t (s) refers to the time for the front of the debris flow to pass the distance and is recorded with a stopwatch. The frontal velocity is used to represent the debris-flow velocity, that is, v = L/t. The flow surface width W (m) refers to the surface width of the front, which is determined based on the field observation data of the cross section before the debris flow breaks out, the marks of the cross-section width, and the mud traces. The flow depth h (m) is the depth of the front. The flow depth of part of the debris flows is measured using ultrasonic sensors (Figure 1b), and the remainder are determined based on cross section marks and mud traces. The bulk density ρ (kg/m³) of each debris flow is determined by sampling at the flow front (Figure 1b). In addition, according to field observations, the flow patterns (surge flow and continuous flow) of the debris flow are recorded.

CHEN ET AL. 4 of 22



Table 1
Information of the 16 July 1999 Debris Flow at Jiangjia Ravine

No.	Flow type	Front time (hh:mm:ss)	Ending time (hh:mm:ss)	Flow depth h (m)	Flow width $W(m)$	Flow velocity v (m/s)	Flow discharge Q (m ³ /s)	Bulk density ρ (kg/m ³)	Total solid concentration φ
1	Continuous flow	01:12:34	01:14:50	0.50	30	8.00	120.0	1,900	0.55
2	Surge flow	01:15:00	01:15:30	0.50	30	8.44	126.6	1,900	0.55
3	Surge flow	01:17:00	01:17:14	0.70	51	8.33	297.4	1,900	0.55
4	Surge flow	01:17:14	01:17:42	0.70	51	7.41	264.5	1,900	0.55
5	Surge flow	01:18:24	01:19:02	0.70	51	6.75	241.0	1,900	0.55
6	Surge flow	01:19:51	01:20:28	0.80	50	6.90	276.0	1,900	0.55
7	Surge flow	01:21:25	01:21:55	1.00	52	8.57	445.6	1,900	0.55
8	Surge flow	01:22:23	01:22:56	1.00	52	8.70	452.4	1,900	0.55
9	Surge flow	01:23:36	01:24:16	0.80	51	7.30	297.8	1,900	0.55
10	Surge flow	01:25:14	01:25:38	0.70	51	7.02	250.6	1,900	0.55
11	Surge flow	01:26:11	01:26:36	1.00	52	9.46	491.9	1,900	0.55
12	Surge flow	01:28:02	01:28:35	0.70	51	7.41	264.5	1,900	0.55
13	Surge flow	01:29:27	01:30:06	0.50	50	7.33	183.2	1,900	0.55
14	Surge flow	01:31:23	01:32:00	0.50	50	6.50	162.5	1,900	0.55
15	Surge flow	01:32:18	01:32:52	0.70	51	7.41	264.5	1,900	0.55
16	Surge flow	01:33:22	01:34:04	1.20	52	7.58	473.0	1,900	0.55
17	Surge flow	01:35:09	01:35:49	1.50	52	7.05	549.9	2,200	0.73
18	Surge flow	01:36:28	01:36:56	0.70	51	5.89	210.3	2,200	0.73
19	Surge flow	01:37:22	01:38:08	0.70	51	6.95	212.4	2,200	0.73
20	Surge flow	01:38:45	01:39:00	0.40	50	5.19	103.8	2,200	0.73
107	Surge flow	06:09:24	06:09:49	0.60	40	3.73	89.5	2,040	0.63
108	Surge flow	06:11:40	06:12:15	0.60	50	5.13	153.9	1,800	0.49
109	Continuous flow	06:15:38	06:17:36	0.60	35	5.19	109.0	1,800	0.49
110	Continuous flow	06:17:36	06:19:08	0.60	30	5.56	100.1	1,800	0.49
111	Continuous flow	06:22:51	06:25:01	0.70	30	6.25	131.2	1,800	0.49
112	Continuous flow	06:25:49	06:26:01	0.60	30	5.67	102.1	2,080	0.66
113	Continuous flow	06:26:49	06:30:01	0.60	30	5.46	98.3	1,870	0.53
114	Continuous flow	06:30:01	06:40:00	0.60	30	6.91	124.4	1,870	0.53
115	Continuous flow	06:40:00	06:41:32	0.40	20	5.10	40.8	1,870	0.53
116	Continuous flow	07:07:03	07:40:00	0.40	10	4.09	16.4	1,870	0.36

When there is an obvious interval between two debris flows, it is regarded as a surge flow. When the continuous discharge is large or the duration of one debris flow is long, it is regarded as a continuous flow.

2.3. Characteristics of Debris Flow at Jiangjia Ravine

In the 93 debris-flow events at Jiangjia Ravine from 1999 to 2017, there were 3,470 surge flows and 582 continuous flows. Information about one debris-flow event as an illustration of the records of an individual event is listed in Table 1.

In DDFORS, a debris-flow event consists of more than a dozen surge flows and several continuous flows (Kang et al., 2004). Based on the on-site ultrasonic measurements, the hydrographs of two debris-flow events (16 July 1999 and 24 July 1999) are shown in Figure 2, reflecting the periodicity of surge flows. The flow patterns of debris flow are controlled by upstream variations in the channel slope. When the sediments stored

CHEN ET AL. 5 of 22

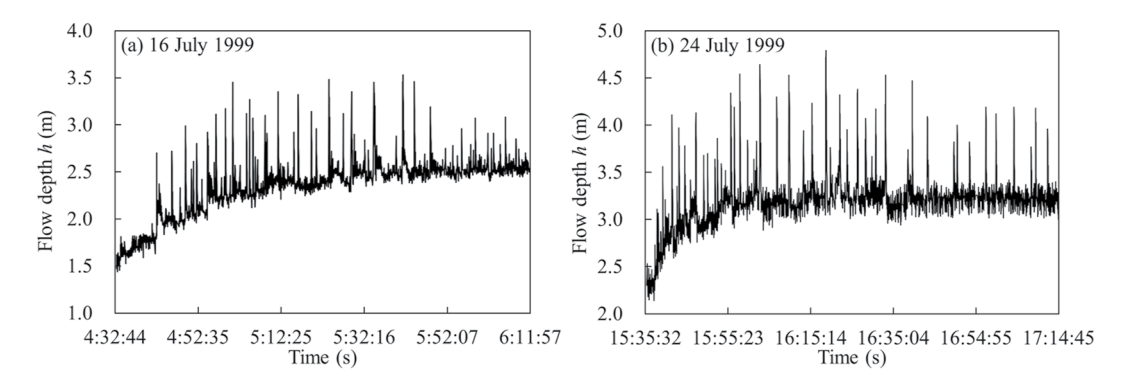


Figure 2. Flow depth hydrograph of surge flows: (a) surge flows on 16 July 1999 and (b) surge flows on 24 July 1999.

in the low-slope section exceed their storage capacity, the channel blockage-breaking effect occurs, and then the discharge of the debris flow suddenly increases, forming a surge flow downstream (Kean et al., 2013). The periodic blockage-breaking effect is an important reason for the formation of surge flow (Guo et al., 2020; Kean et al., 2013). A typical surge flow (Figure 1b) shows a steep front with the densest slurry and the highest concentration of particles, followed by a tail where the solid concentration gradually becomes diluted and the flow depth becomes shallower (Iverson, 1997; McArdell et al., 2007). The wide gradation is also one of the obvious characteristics of Jiangjia Ravine debris flows. The particle size ranges from 10^{-6} –10 m, the bulk density is between 1,600 and 2,300 kg/m³, and the total solid concentration is as high as 0.85 (Cui et al., 2005).

Surge flow and continuous flow show distinct differences in material composition and flow regimes. The debris materials were sampled and sieved, and the particle size distribution curves of surge flows and continuous flows were obtained (Figure 3). The average particle size distribution curves of surge flows and continuous flows are shown in Figures 3a and 3b, respectively. The insets show the particle size distribution curves of 16 surge flows and 16 continuous flows. In the particle size range of 0.5–100 mm, the particle size distribution curves of surge flows are steeper than those of continuous flows, and the sorting is poor. The important reason why debris flow cannot be regarded as a simple Newtonian fluid is that the fluid phase of debris flow is not water but a slurry composed of fine particles (clay and silt) and water. Slurry plays an indispensable role in the movement of debris flow (Coussot, 1995; Fei et al., 1991; Kaitna et al., 2016). Thus, determining the critical particle size between the solid phase and the fluid phase becomes a fundamental problem.

The critical particle size is a characterization of the suspension competence of a debris flow (Pierson, 1981). During the movement of a debris flow, the critical particle size varies with the flow regime. In a fast-flowing state, larger particles are suspended and move together with the fluid, being treated as a slurry. Therefore, for a debris flow with a wide gradation in nature, the critical particle size should be determined cautiously. In DDFORS, it was found that the solid mass content of particles <2 mm generally does not vary with the total solid concentration (approximately 680 kg/m³, (Fei et al., 1991)), indicating that particles <2 mm could be regarded as slurry. In this study, the critical particle size of the debris flow was 1.2 mm, as suggested by Cui et al. (2005). In the following analysis, the solid concentration φ_s excludes fine particles with a particle size of less than 1.2 mm.

Since fine particles below 1.2 mm are considered the fluid phase, the median diameters of solid particles d_{50} in surge and continuous flows are 12 and 6 mm, respectively, regarded as the characteristic diameters δ . For surge flows, the d_{60} and d_{10} of particles are 17 and 2 mm, and for continuous flow, the d_{60} and d_{10} of particles are 7.6 and 1.7 mm, respectively (Figure 3). The nonuniform coefficients (d_{60}/d_{10}) of particles of surge flows and continuous flow are 8.5 and 4.5, respectively, which indicates that the solid particles of Jiangjia Ravine debris flows are nonuniform, especially for the surge flows.

The parameters of the Jiangjia Ravine debris flows used in this study are summarized in Table 2. For the 3,470 surge flows, the range of flow depth is 0.1–3.0 m, and the range of flow velocity is 1.7–14.3 m/s. For the 582 continuous flows, the range of flow depth is 0.2–2.0 m and the range of flow velocity is 1.6–14.0 m/s. The viscosity of interstitial fluid varies by several orders of magnitude, from water (10^{-3} Pa·s) to a slurry composed of fine particles (10^{1} Pa·s) (Coussot, 1995; Hsu et al., 2014; Sosio & Crosta, 2009; Sosio et al., 2007). Rheological tests show that the ranges of viscosity η of surge flows and continuous flows are 0.14–5.61 and 0.05–4.66 Pa·s,

CHEN ET AL. 6 of 22

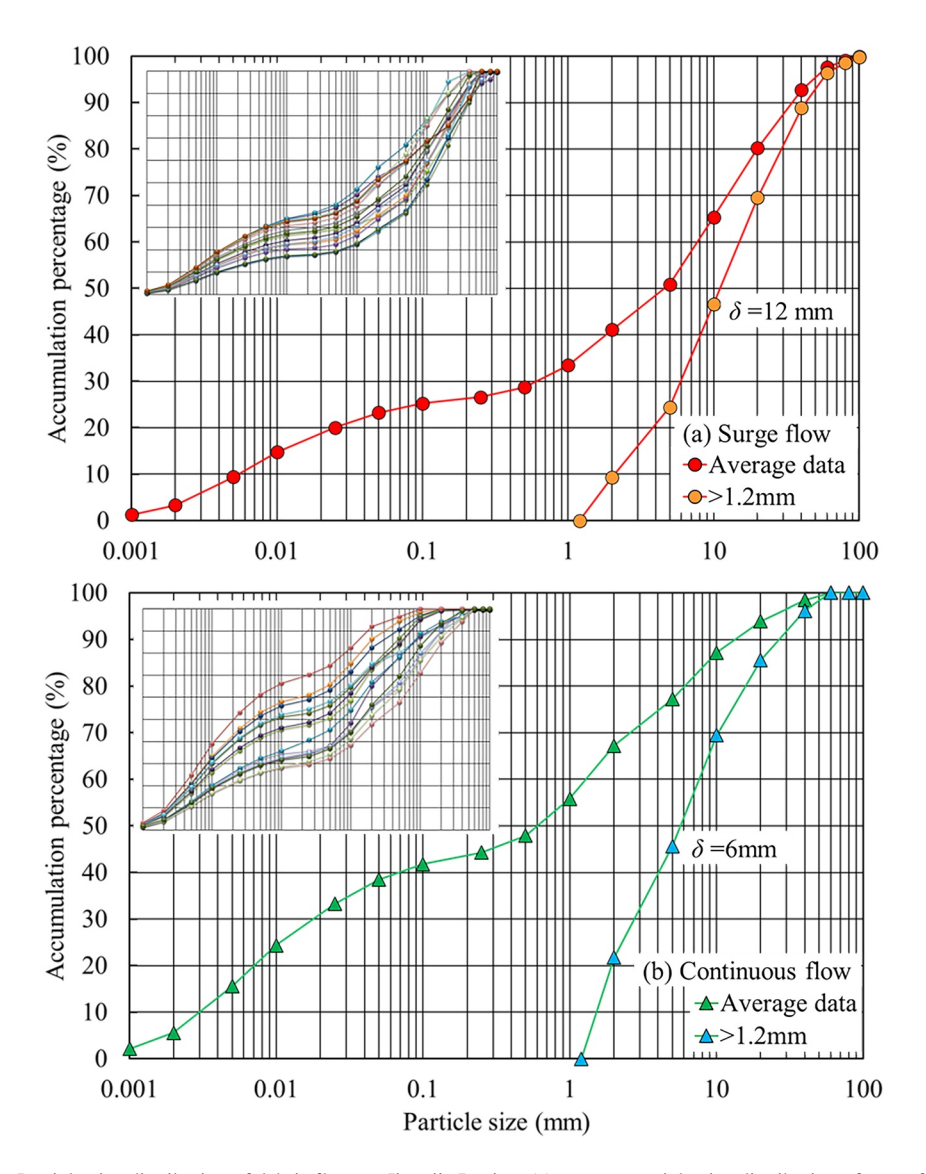


Figure 3. Particle-size distribution of debris flows at Jiangjia Ravine: (a) average particle-size distribution of surge flows and (b) average particle-size distribution of continuous flows. The insets in panels (a and b) show the particle-size distribution curves of 16 surge flows and 16 continuous flows, respectively.

respectively. The internal friction angle ϕ of the solid particles is 29.8° (Kang et al., 2004), and the density of solid particles ρ_s is 2,650 kg/m³.

2.4. Manning's Coefficient of Debris Flows at Jiangjia Ravine

For the field observation data of the 93 debris-flow events, the variations in flow depth h and velocity v against solid concentration φ_s are shown in Figure 4. The flow depth and flow velocity are positively correlated with the solid concentration. Moreover, the flow depth and velocity of surge flows are generally higher than those of continuous flows, and are distributed in the range of higher solid concentrations.

Based on the flow depths and flow velocities of the 93 debris-flow events, Manning's coefficient n is back-calculated (Equation 2). For surge flows, the range of Manning's coefficient n is 0.01–0.08, with an average of 0.03. For continuous flows, the range of Manning's coefficient n is 0.01–0.13, also with an average of 0.03. The variation in Manning's coefficient n with flow depth n is shown in Figure 5. Manning's coefficient increases with increasing flow depth. Under the fixed channel conditions (only the Jiangjia Ravine considered), combined with the positive correlation between flow depth and solid concentration (Figure 4b), Figure 5 indicates that Manning's coefficient

CHEN ET AL. 7 of 22

Table 2 Parameters of Surge Flows and Continuous Flows							
Parameters	Surge flow	Continuous flow					
Density of solid particles $\rho_{\rm s}$ (kg/m ³)	2,650	2,650					
Bulk density ρ (kg/m ³)	1,600–2,390	1,360-2,350					
Fluid density $\rho_{\rm f}$ (kg/m ³)	1,275–2,076	1,230–2,193					
Fluid viscosity η (Pa·s)	0.14-5.61	0.05-4.66					
Volumetric solid concentration of coarse grain φ_s	0.24-0.55	0.10-0.34					
Volumetric solid concentration of fines ϕ_{f}	0.13-0.30	0.13-0.47					
Characteristic diameter δ (m)	0.012	0.006					
Flow depth h (m)	0.1-3.0	0.2-2.0					
Velocity v (m/s)	1.7–14.3	1.6–14.0					
Slope angle θ (°)	3.7	3.7					
Stokes number St	0.5-91.1	0.2–32.3					
Bagnold number $N_{\rm B}$	0.5–28.3	0.1-5.3					
Density ratio r	1.1–1.4	1.0–1.5					

varies with the physical properties of debris flow, for example, the internal shear rate and solid concentration. The internal resistance is proven to be the main source of the flow resistance (Cui et al., 2016). Therefore, it is imperative to further analyze the flow resistance from the perspective of the physical mechanisms of debris flow.

2.5. State of Liquefaction of Debris Flows at Jiangjia Ravine

The slope of the field observation section is approximately 3.7° in DDFORS. However, on such a gentle slope, there are debris flows with velocities higher than 10 m/s. An obvious reason is the state of liquefaction (When the pore fluid pressure is equal to the total normal stress, the effective stress disappears fully and the solid-fluid mixture behave like a liquid). The pore fluid pressure in a debris flow can remain elevated well above the hydrostatic pressure levels. In other words, excess pore fluid pressure is generated to maintain the debris flow in a nearly liquefied state and leads to lower flow resistance. The Darcy number N_{Dar} can be used to describe the maintenance of excess pore fluid pressure, which is expressed as the ratio of the solid-fluid interaction stress to the particle collisional stress (Iverson, 1997; Lanzoni et al., 2017)

$$N_{\text{Dar}} = \frac{\eta}{\varphi, \rho, \dot{\gamma} k} \tag{3}$$

where $\dot{\gamma}$ is the average shear rate (1/s), for viscous flows, $\dot{\gamma} = 3v/2h$, and for inertial flows, $\dot{\gamma} = 5v/3h$ (Cassar et al., 2005); k is the hydraulic permeability of the sediments (m²), which is related to the solid concentration and its empirical expression is

$$k(\phi_s) = k_0 \exp\left(\frac{0.60 - \phi_s}{0.04}\right)$$
 (4)

For natural debris flows, the reference permeability k_0 ranges from 10^{-10} to 10^{-13} m² (Iverson & George, 2014), and k_0 is taken as 10^{-12} m² in this study. According to Equation 4, the hydraulic permeability of sediments in Jiangjia Ravine is 3.7×10^{-12} – 3.6×10^{-9} m². Adopting Equation 3, the range of Darcy numbers of Jiangjia Ravine debris flows is 6.3×10^{1} – 9.8×10^{9} . The Darcy number increases with increasing solid concentration (Figure 6a). Debris flows with solid concentrations lower than 0.40 are close to liquefaction (Iverson, 1997; Song et al., 2021); obviously, debris flows with solid concentrations of approximately 0.10 are liquefied. However, to preserve the integrity of the field observation data of the Jiangjia Ravine debris flows, debris flows in the entire solid concentration range (0.10–0.55) is considered in the analysis of the liquefaction state. For debris flows with a high fraction of fines, the excess pore fluid pressure is significant, which is characterized by $N_{\rm Dar} > 50$ –60 (Lanzoni et al., 2017). The high Darcy number indicates that the Jiangjia Ravine debris flows show high excess pore fluid pressure and are close to liquefaction.

CHEN ET AL. 8 of 22

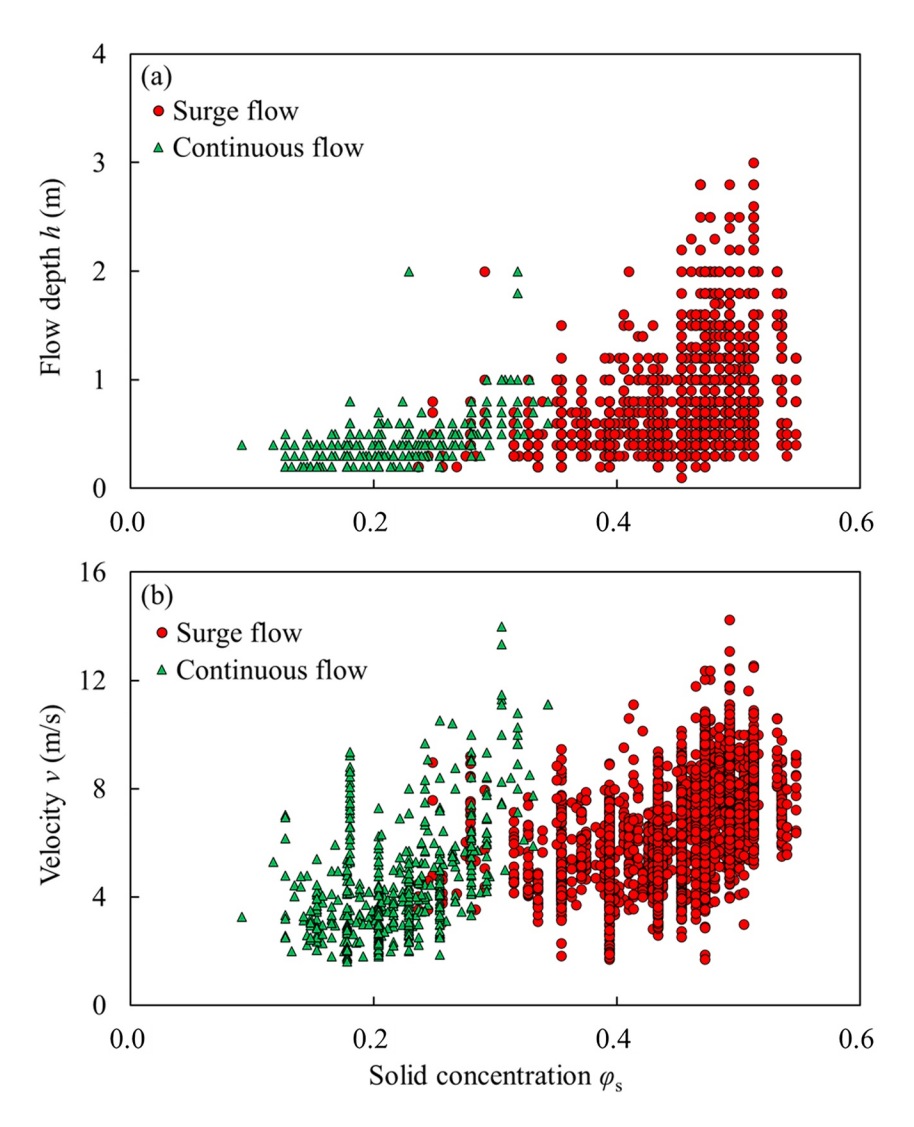


Figure 4. Flow depth and velocity of surge flows and continuous flows at different solid concentrations: (a) flow depth and (b) velocity.

The liquefaction ratio is defined as the ratio of the pore fluid pressure P to the normal stress σ , that is, $LR = P/\sigma$. When LR is close to unity, it indicates that the debris flow is in a completely liquefied state. Equation 5, which

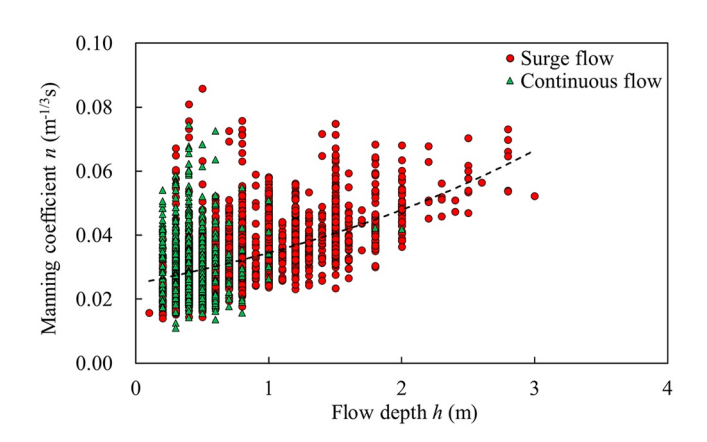


Figure 5. Relationship between Manning's coefficient and flow depth.

considers the contributions of both solid phase frictional and fluid phase viscous effects, is a common formula for the flow resistance of debris flow (Ancey, 2007; Ancey & Evesque, 2000; Rauter et al., 2016), and it can be used to estimate the liquefaction ratio LR (Hungr, 1995; Hungr & McDougall, 2009).

$$\tau = \mu_{\rm p} \sigma_{\rm e} + \dot{\gamma} \eta \tag{5}$$

where μ_p is the friction coefficient of particles, $\mu_p = \tan \phi$, ϕ is the internal friction angle of solid particles, and $\sigma_e = \sigma - P$ represents the effective stress (Pa), for steady flow, $\sigma = \rho gh \cos \theta$. In Equation 5, $\mu_p \sigma_e$ is the resistance provided by particle contact friction, indicating that flow resistance is related to effective stress; $\dot{\gamma}\eta$ is the contribution of the fluid viscous effect to the flow resistance, which depends on the shear rate. By substituting the above relations into Equation 5, the liquefaction ratio LR of debris flow can be deduced from a back-of-the-envelope approach.

CHEN ET AL. 9 of 22

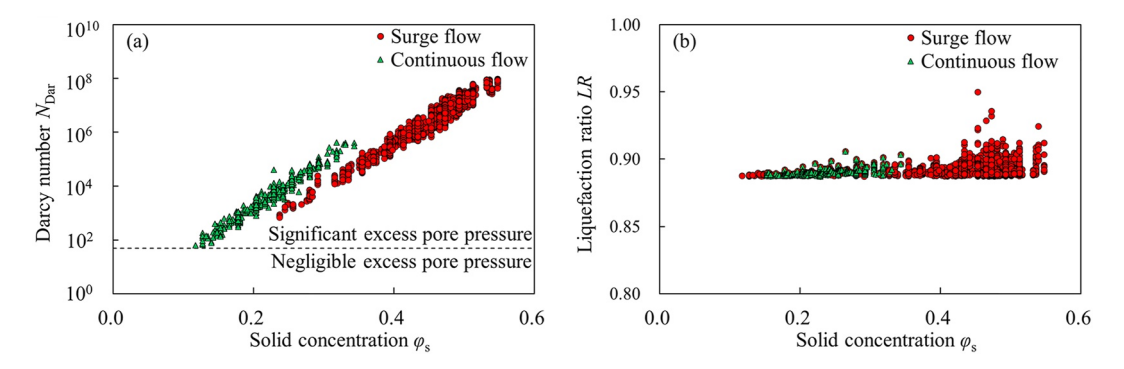


Figure 6. The liquefaction ratio of Jiangjia Ravine debris flows: (a) relationship between Darcy number and solid concentration and (b) deduced the lower limits of liquefaction ratio.

$$LR = 1 + \frac{\dot{\gamma}\eta}{\mu_{\rm p}\rho_{\rm g}h\cos\theta} - \frac{\tan\theta}{\mu_{\rm p}} \tag{6}$$

Note that the contribution of collisional force is not considered. In other words, the contribution of frictional stress (effective stress) is exaggerated in Equation 5. Therefore, the liquefaction ratio calculated by Equation 6 should be the lower limit. According to Equation 6, for Jiangjia Ravine debris flows, the range of liquefaction ratio is 0.89–0.95, indicating that the debris flows are close to liquefaction (Figure 6b). Under the premise of considering the effective stress, the calculated liquefaction ratio is still very high, that is, close to unity, indicating that the state of debris flow is close to be fully liquefied. Based on the above two arguments, the contribution by particle contact friction is not the main source of flow resistance. Therefore, the main source of flow resistance under such a gentle slope remains unclear at Jiangjia Ravine. This problem will be explained in detail in the next section.

3. Flow Regime and Flow Resistance of Debris Flow

3.1. Flow Regime of Debris Flow at Jiangjia Ravine

In the framework of traditional rheology ($\tau = \eta_s(\varphi_s)\eta\dot{\gamma}$), geophysical flows are regarded as equivalent fluids, and rheological properties only depend on the solid concentration. Increasing the solid concentration enhances the viscosity of a fluid (Batchelor & Green, 1972; Einstein, 1905; Stickel & Powell, 2005). Traditional rheology is only applicable to single-phase flow, in which particles and fluid move together at the same average veloc-

ity. However, in many flow configurations, there is obvious relative motion between particles and fluid, and debris flow is a typical example.

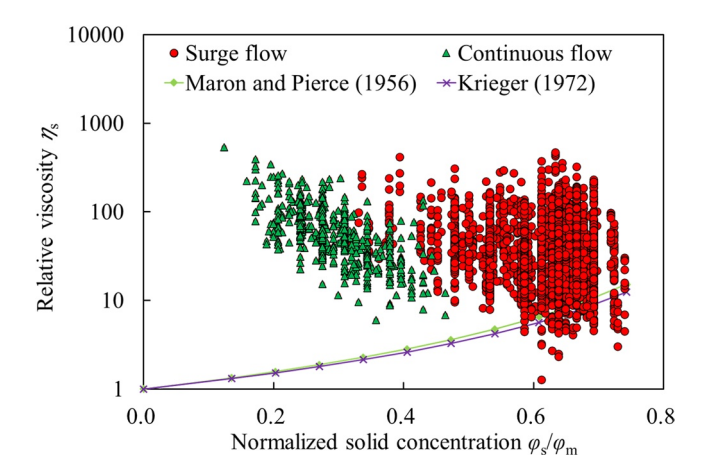


Figure 7. Relationship between relative viscosity and normalized solid concentration of Jiangjia Ravine debris flows. Viscosity laws: $\eta_s = (1 - \varphi_s/\varphi_m)^{-2}$ (Maron & Pierce, 1956), $\eta_s = (1 - \varphi_s/\varphi_m)^{-2\varphi_m}$ (Krieger, 1972).

In DDFORS, the natural setting of a straight channel with a slope of 3.7° can be regarded as an inclined plate rheometer to explore the rheological characteristics of debris flows. For traditional rheology, the performance of the two viscosity laws (Krieger, 1972; Maron & Pierce, 1956) is evaluated. Figure 7 shows the relationship between the relative viscosity $\eta_s (= \tau/\eta\dot{\gamma})$ and the normalized solid concentration φ_s/φ_m . The maximum solid concentration φ_m of the Jiangjia Ravine debris flow is approximately 0.74 (Yang et al., 2012).

The dependence of the relative viscosity η_s on the normalized solid concentration φ_s/φ_m is not obvious for Jiangjia Ravine debris flows (Figure 7). There is a large deviation on the low-concentration side, where the velocity and shear rate are both high. The two viscosity laws of Krieger (1972) and Maron and Pierce (1956) regard debris flows as equivalent fluids, regardless of the interactions between particles or between particles and fluid. In other words, the fluid viscous drag is the source of flow resistance. However, for natural debris flows, both the fluid viscous effect and particle interaction contribute to the flow resistance (McArdell et al., 2007; Nagl et al., 2020). Therefore,

CHEN ET AL. 10 of 22

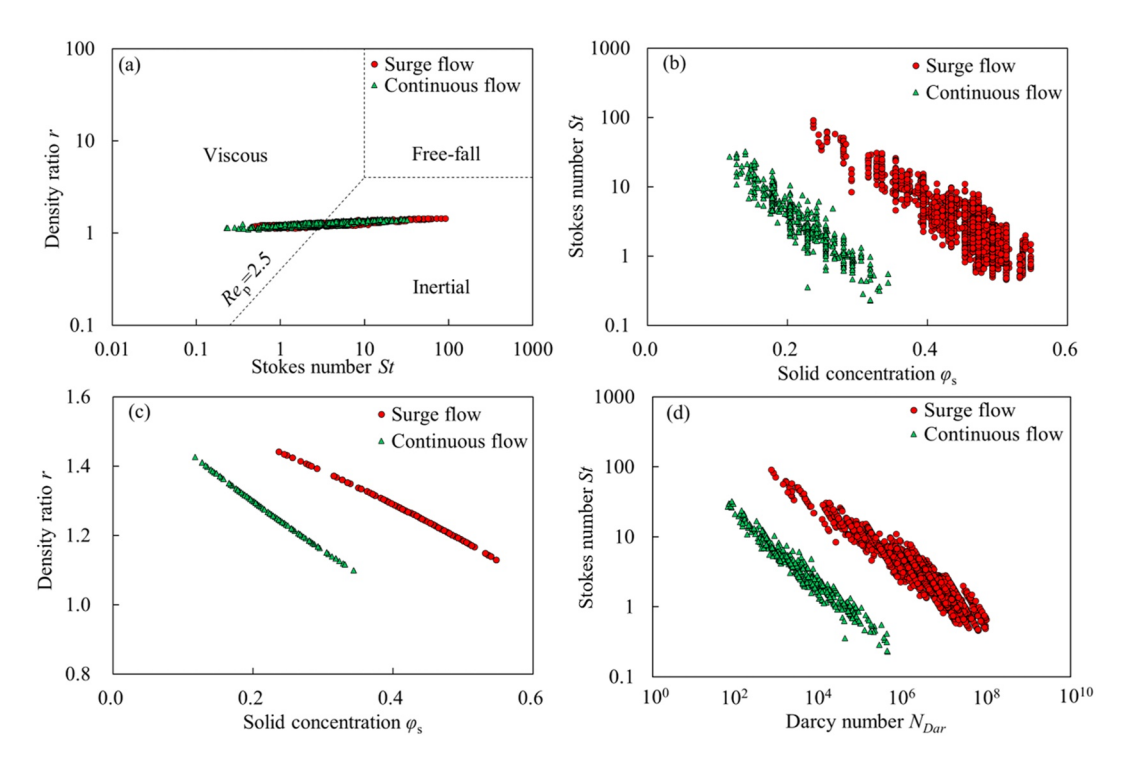


Figure 8. Flow regimes of Jiangjia Ravine debris flows: (a) flow regimes in (St, *r*) space; (b) relationship between Stokes number and solid concentration; (c) relationship between density ratio number and solid concentration; and (d) relationship between Stokes number and Darcy number.

the equivalent-fluid approach cannot explain the dynamic characteristics of debris flow, and the solid-fluid interaction must be explicitly considered.

The solid-fluid interaction in debris flows, that is, the coupling among the particle contact friction, instantaneous collision (inertia) and hydrodynamic effects of fluid viscosity, is the key to studying debris-flow dynamics (Boyer et al., 2011; Iverson, 2000; Trulsson et al., 2012). There are three time scales for particle motion: free-fall, inertial, and viscous. These three time scales correspond to the three regimes of free fall, inertial, and viscous and are distinguished by the Stokes number St, the density ratio r, and the particle Reynolds number Re_p (Cassar et al., 2005; Courrech du Pont et al., 2003). The Stokes number St is defined as the ratio of particle inertia to the fluid viscous effect:

$$St = \frac{\rho_s \dot{\gamma} \delta^2}{\eta} \tag{7}$$

The Stokes number St represents the ability of particles to follow a fluid. The lower the St is, the stronger the following trend of particles. The density ratio is expressed as follows:

$$r = \sqrt{\frac{\rho_s}{\rho_f}} \tag{8}$$

where $\rho_{\rm s}$ is the density of the solid particles and $\rho_{\rm f}$ is the fluid density (kg/m³).

As shown by Courrech du Pont et al. (2003), for St <<1, r>>1, a viscous regime where the particle reaches the viscous limit velocity during the motion of the particle. For St >>1, r<<1, an inertial regime where the particle reaches the inertial limit velocity. For St >>1, r>>1, a free-fall regime where the particle follows an accelerated motion. Density ratio r=4 separates the free-fall and inertial regimes, and Stokes number St = 10 separates the free-fall and viscous regimes (Courrech du Pont et al., 2003). The boundary between particle inertia and the fluid viscous effect is determined by Re_p = St/r=2.5, where Re_p <2.5 is the viscous regime and Re_p >2.5 is the inertial regime (Courrech du Pont et al., 2003). According to the thresholds of Stokes number St, density ratio r, and the particle Reynolds number, the flow regimes of surge flows and continuous flows are shown in Figure 8a.

CHEN ET AL. 11 of 22

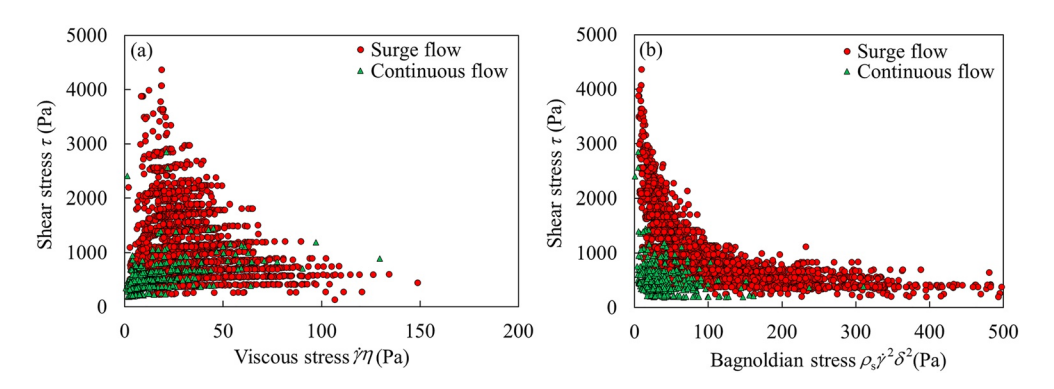


Figure 9. Relationships between flow resistance and internal stresses: (a) viscous stress and (b) Bagnoldian stress.

In Figure 8a, the flow regimes of the Jiangjia Ravine debris flows spread in the viscous and inertial regions, indicating that the flow regime of natural debris flows is not dominated by either viscous or particle inertial effects. Instead, as the solid concentration and viscosity vary, the flow regime gradually transitions from the viscous to particle inertial effects, and there is a continuous transition between these two flow regimes.

As elaborated in Section 2.5, either for surge flows or continuous flows, the particle contact friction contributed by effective stress is negligible. Moreover, in the (St, r) space, the flow regime of a debris flow varies from viscous to inertial. Therefore, it can be inferred that the flow resistance of the Jiangjia Ravine debris flow is weakly related to particle contact friction ($\mu_n \sigma_n$) but comes from the fluid viscous effect and inertial collision.

3.2. Visco-Collisional Scaling Law of Debris-Flow Resistance

In the viscous regime, the viscosity of the slurry is recognized as the main source of flow resistance, that is, $\tau \sim \dot{\gamma}\eta$. In the inertial regime, the flow resistance is caused by particle collisions, and the shear stress is proportional to the square of the shear rate and characteristic particle size, that is, the Bagnoldian scaling: $\tau \sim \rho_S \dot{\gamma}^2 \delta^2$. With increasing solid concentration, the Strokes number St decreases (Figure 8b). This indicates that for debris flows with high solid concentrations, the volumetric concentration of fine particles (clay and silts) is relatively high, and the fluid-phase viscosity tends to dominate (low St). Since the density of solid particles is constant $(\rho_s = 2,650 \text{ kg/m}^3)$, the density ratio decreases with an increase in the solid concentration, which means that the increase in the solid concentration helps to increase the fine particle content and can increase the fluid density (Figure 8c). As the Darcy number $N_{\rm Dar}$ increases, the Stokes number St decreases, indicating that the excess pore pressure can buffer particle collisions (Figure 8d). These results indicate that the slurry attenuates particle collision through fluid viscous damping, the inertial effect, and the maintenance of high excess pore pressure, so that solid particles and fluid tend to move together. In addition, the suspension competence of fluid increases with increasing fine content (Pierson, 1981), which makes some settled clasts become neutrally suspended particles. For debris flows dominated by inertial collision, the suspension competence of the fluid is reduced. The following of particles to fluid is weak, which makes the relative motion between the solid and fluid phases obvious, and particle collisions become intense.

The flow regime of a debris flow depends on the relative magnitudes of the viscous and inertial stresses. Assuming steady flow conditions, the relationships between flow resistance τ (= $\rho gh \sin \theta$) and viscous stress $\dot{\gamma}\eta$ and particle collisional stress $\rho_S \dot{\gamma}^2 \delta^2$ are plotted in Figure 9a and Figure 9b, respectively. The data points are highly scattered, and there is no unique relationship between the flow resistance and the calculated internal stresses. The flow resistance shows an increasing trend with increasing viscous stress (Figure 9a). The more significant the particle collisions are, the lower the flow resistance. In surge flows, this decreasing trend is even obvious (Figure 9b). This means that neither the viscous effect nor the collisional effect alone can unify the flow resistance of the Jiangjia Ravine debris flow.

Dimensional analysis shows that the solid-fluid interaction of debris flow can be quantified by dimensionless parameters consisting of two physical effects, namely, viscous stress and collisional stress (Iverson, 1997). The Stokes number shows a clear physical meaning and can be used to divide the flow regime. However, the Stokes number does not consider the effect of the solid concentration. To fully consider the two-phase flow

CHEN ET AL. 12 of 22

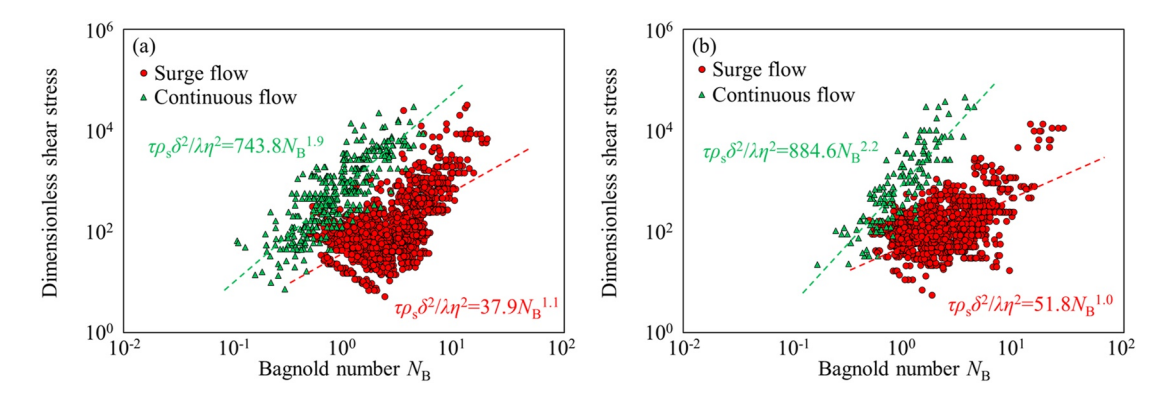


Figure 10. Relationship between dimensionless shear stress and Bagnold number: (a) obtained from the observation data from 1999 to 2001; (b) the relationship in panel (a) verified by the 2002–2017 debris flow observation data.

characteristics affected by the physical composition, the Bagnold number $N_{\rm B}$ is further used to quantify the contribution of solid-fluid interaction to flow resistance. The expression of the Bagnold number $N_{\rm B}$ is as follows:

$$N_{\rm B} = \frac{\lambda \rho_{\rm s} \dot{\gamma} \delta^2}{n} \tag{9}$$

where $\lambda = \varphi_s/(1 - \varphi_s)$. From Equation 9, the Bagnold number can be regarded as a modified Stokes number.

Based on the observation data of 34 debris-flow events (1,844 surge flows and 433 continuous flows) from 1999 to 2001, the relationship between the dimensionless shear stress $\tau \rho_s \delta^2 / \lambda \eta^2$ and Bagnold number N_B of surge flows and continuous flows is obtained (Figure 10a). As more data points concentrate in the lower range of N_B , the fitted line of surge flows deviates from its apparent trend. A strong correlation between dimensionless shear stress and Bagnold number is found

$$\tau \rho_{\rm s} \delta^2 / \lambda \eta^2 = a N_{\rm B}^b \tag{10}$$

Based on Equation 10, the relationship between shear stress and the Bagnold number can be further obtained, that is, the visco-collisional scaling law

$$\tau = a \left(\frac{\lambda \eta^2}{\rho_{\rm s} \delta^2} \right) N_{\rm B}^b \tag{11}$$

Both a and b are fitted constants. Equation 11 is further verified by the observation data of 59 debris-flow events (1,626 surge flows and 149 continuous flows) from 2002 to 2017. As shown in Figure 10b, although the fitting coefficients a and b are not exactly the same as those in Figure 10a (this might be affected by the scattered field data), the trend of the fitting expressions of 59 debris-flow events from 2002 to 2017 are close to those in Figure 10a, which proves that visco-collisional scaling law (Equation 11) is appropriate for predicting the flow resistance of natural debris flows. Substituting the expression of the Bagnold number (Equation 9) into Equation 11, this relationship can be further expressed as

$$\tau = a \left(\frac{\lambda^{1+b} \eta^2}{\rho_s \delta^2} \right) \left(\frac{\rho_s \dot{\gamma} \delta^2}{\eta} \right)^b$$

$$= a \lambda^{1+b} \dot{\gamma}^b \eta^{2-b} \rho_s^{b-1} \delta^{2(b-1)}$$
(12)

For Equation 12, when b=1, $\tau=a\lambda^2\dot{\gamma}\eta$, the flow resistance is fully contributed by the viscous stress, that is, $\tau\sim\dot{\gamma}\eta$. When b=2, $\tau=a\lambda^3\rho_s\dot{\gamma}^2\delta^2$, the flow resistance is fully dominated by the collisional stress, that is, $\tau\sim\rho_s\dot{\gamma}^2\delta^2$. For surge flows, b=1.1, indicating that the flow resistance mainly comes from the viscous effect. For continuous flows, b=1.9, indicating that the flow resistance is mainly dominated by particle collisional stress (Figure 10). Therefore, b is in the range of viscous flows (b=1) and Bagnoldian flows (b=2), indicating that both viscous effect and particle collisions contribute to the flow resistance, but the contributions of these two stresses differ. In other words, for Jiangjia Ravine debris flows, the visco-collisional effect becomes the main mechanism of solid-fluid interaction (Song et al., 2021) rather than the sustained contact friction in experimental dense two-phase flows (Iverson, 2000; Pailha & Pouliquen, 2009).

CHEN ET AL. 13 of 22



The above analysis indicates that the flow regimes of Jiangjia Ravine debris flow are distributed in both viscous and inertial regions. Adopting the 34 debris-flow events from 1999 to 2001, a visco-collisional scaling law is proposed. Based on the verification using 59 debris-flow events from 2002 to 2017, it is proved that this law is suitable for predicting the flow resistance of natural debris flows. In addition, in this law, the constant *b* is essential as it provides the physical meaning to the flow type.

4. The Empirical Description of Flow Resistance With Physical Mechanisms

4.1. The Empirical Description of Flow Resistance

Jiangjia Ravine debris-flow observation data come from a straight rectangular channel. Assuming that debris flow is a steady and uniform flow, an empirical description of the flow resistance of open channel flow is adopted. Manning's formula characterizing flow resistance with a comprehensive roughness coefficient has been widely used. The bed slope S derived from Manning's formula (Equation 2) is

$$S = \frac{v^2 n^2}{h^{4/3}} \tag{13}$$

By substituting Equation 13 into Equation 1, the relationship between flow resistance τ and Manning's coefficient n can be expressed (Bellos et al., 2018; Hungr & McDougall, 2009)

$$\tau = \frac{\rho g v^2 n^2}{h^{1/3}} \tag{14}$$

For debris flows, flow resistance is not only affected by channel boundary conditions but also controlled by solid-fluid interactions (Cui et al., 2016). Thus, Manning's coefficient should include both the external factors (channel boundary conditions) and the intrinsic dynamics of debris flow. However, Manning's formula reflects the dynamic characteristics of debris flow by defining the comprehensive roughness coefficient, which obscures external and internal factors and thus is not conducive to further understanding the flow resistance. Introducing physical mechanisms could compensate for the deficiency of Manning's formula in terms of clear physical meaning.

4.2. Manning Formula Modified by the Visco-Collisional Scaling Law

The purpose of this section is to introduce the flow resistance model with physical mechanisms into the empirical formula of flow resistance. The debris-flow field observation data used in this study are from the same site, so the effect of channel roughness on the flow resistance is fixed. Under this premise, the physical mechanisms of flow resistance can be further combined with empirical descriptions to fully reflect the dynamic characteristics of debris flow. Combining Equation 11 with Equation 14, the relationship between Manning's coefficient n and the Bagnold number N_B is derived

$$n = \left(\frac{ah^{1/3}\lambda\eta^2}{\rho_s\rho\delta^2v^2g}\right)^{1/2}(N_{\rm B})^{b/2} \tag{15}$$

Equation 15 adopts the Bagnold number $N_{\rm B}$, which characterizes the visco-collisional effect of debris flow, to unify the physical mechanisms and empirical description of flow resistance. For one debris-flow event, the parameters representing the intrinsic properties of the debris flow (bulk density ρ , density of solid particles $\rho_{\rm s}$, solid concentration $\varphi_{\rm s}$, viscosity η , and characteristic particle size δ) are known. Flow depth h and flow velocity v need to be measured or estimated on site. The Bagnold numbers $N_{\rm B}$, a, and b can be obtained from these determined physical parameters. Then, combined with the field-observed flow depth h and velocity v, the flow resistance of the debris flow can be determined.

Under fixed channel boundary conditions, Equation 15 indicates that Manning's coefficient is controlled by the flow regime of the debris flow, and its value can be determined by the intrinsic properties of the debris flow, which provides a basis for practical applications. To illustrate this comprehensive effect intuitively, Manning's coefficient is calculated by adopting the typical values of the parameters involved in Equation 15. The values of flow depth h are 0.1, 1, 10, and 100 m (for illustration purposes only). The values of flow velocity v are 1, 8, and 15 m/s. The range of fluid viscosity η varies from water to slurry: 0.001, 0.01, 0.1, and 1 Pa·s. The remaining parameters are listed in Table 3. In Figure 11, the planes constructed by flow depth h, flow velocity v, and fluid viscosity η are the theoretical relationship between Manning's coefficient n and the Bagnold number N_B , that is,

CHEN ET AL. 14 of 22

Table 3 Parameters for the Theoretical Planes of Manning's Coefficient n and Bagnold Number N_B							
Density of solid particles ρ_s (kg/m ³)	2,650	2,650					
Bulk density ρ (kg/m ³)	2,146	1,858					
Fluid density $\rho_{\rm f}$ (kg/m ³)	1,744	1,647					
Fluid viscosity η (Pa·s)	0.001, 0.01, 0.1, 1	0.001, 0.01, 0.1, 1					
Volumetric solid concentration of coarse grain $\varphi_{\rm s}$	0.45	0.22					
Characteristic diameter δ (m)	0.012	0.006					
Flow depth h (m)	0.1, 1, 10, 100	0.1, 1, 10, 100					
Velocity v (m/s)	1, 8, 15	1, 8, 15					
Bagnold number $N_{\rm B}$	$4.7 \times 10^{-5} - 7.8 \times 10^{5}$	$3.9 \times 10^{-6} - 6.5 \times 10^{4}$					
Constant a	37.9	743.8					
Constant b	1.1	1.9					

 $n(N_{\rm B})$, which are the visual representations of Equation 15. The theoretical planes of $n(N_{\rm B})$ with velocities of 1, 8, and 15 m/s are plotted separately for surge flows (Figures 11a–11c) and continuous flows (Figures 11d–11f). These theoretical planes show the upper and lower limits of Equation 15 and cover the range of debris flow in natural settings. It is apparent that Manning's coefficient could be a result of different combinations of debris flow parameters.

In addition, the field data of 59 debris-flow events from 2002 to 2017 also confirm the comprehensive effect of Equation 15. In Figure 11, the red and green data points show the relationship between Manning's coefficient n and the Bagnold number N_B of surge flows and continuous flows, respectively. For surge flows, Manning's coefficient decreases with increasing Bagnold number. Nevertheless, this does not indicate a linear relationship between Manning's coefficient and the Bagnold number. Empirical curve fitting does not reflect the physical mechanisms. Rather, from Equation 15, Manning's coefficient is affected by the intrinsic properties of debris flow. The calculated Manning's coefficients of Jiangjia Ravine debris flows fall within the theoretical planes of $n(N_B)$, validating the predictability of Equation 15.

Furthermore, by substituting Manning's coefficient $n(N_B)$ (Equation 15) into Manning's formula (Equation 2), the expression of flow velocity can be obtained:

$$v = \left[\frac{(\rho g S)^{1/2} \rho_s^{(1-b)/2} \delta^{1-b} \eta^{1-2/b}}{a^{1/2} \lambda^{(1+b)/2}} \right]^{2/b} h^{(1+b)/b}$$
 (16)

Despite its complexity, Equation 16 demonstrates that, since the physical quantities within the square brackets are known, flow velocity v is solely a function of flow depth h. Once the flow depth h is obtained from real-time observation or postevent survey, the flow velocity can be calculated accordingly. The flow velocities of 59 debrisflow events from 2002 to 2017 were calculated using Equation 16. Figure 12 shows the relationship between the calculated velocities v_n and the observed velocities v. The field observation data of debris flow are scattered, and the calculated velocities generally match the observed velocities.

In summary, under the same channel boundary conditions, the visco-collisional scaling law is introduced into the empirical equation of flow resistance, and a relationship between the Manning coefficient and Bagnold number is established. This relationship shows that the Manning coefficient is related to the flow regime of debris flow, which gives the Manning coefficient a clear physical meaning.

5. Discussion

5.1. The Discreteness of Field Observation Data

The essential value of the field observation data is that it is free of the scale effect, but there is inevitable discreteness, for example, in the measured flow depth and velocity (Figure 4). The spreading of the fundamental observation parameters was further transferred to the relevant deduced parameters, such as Manning's coefficient

CHEN ET AL. 15 of 22

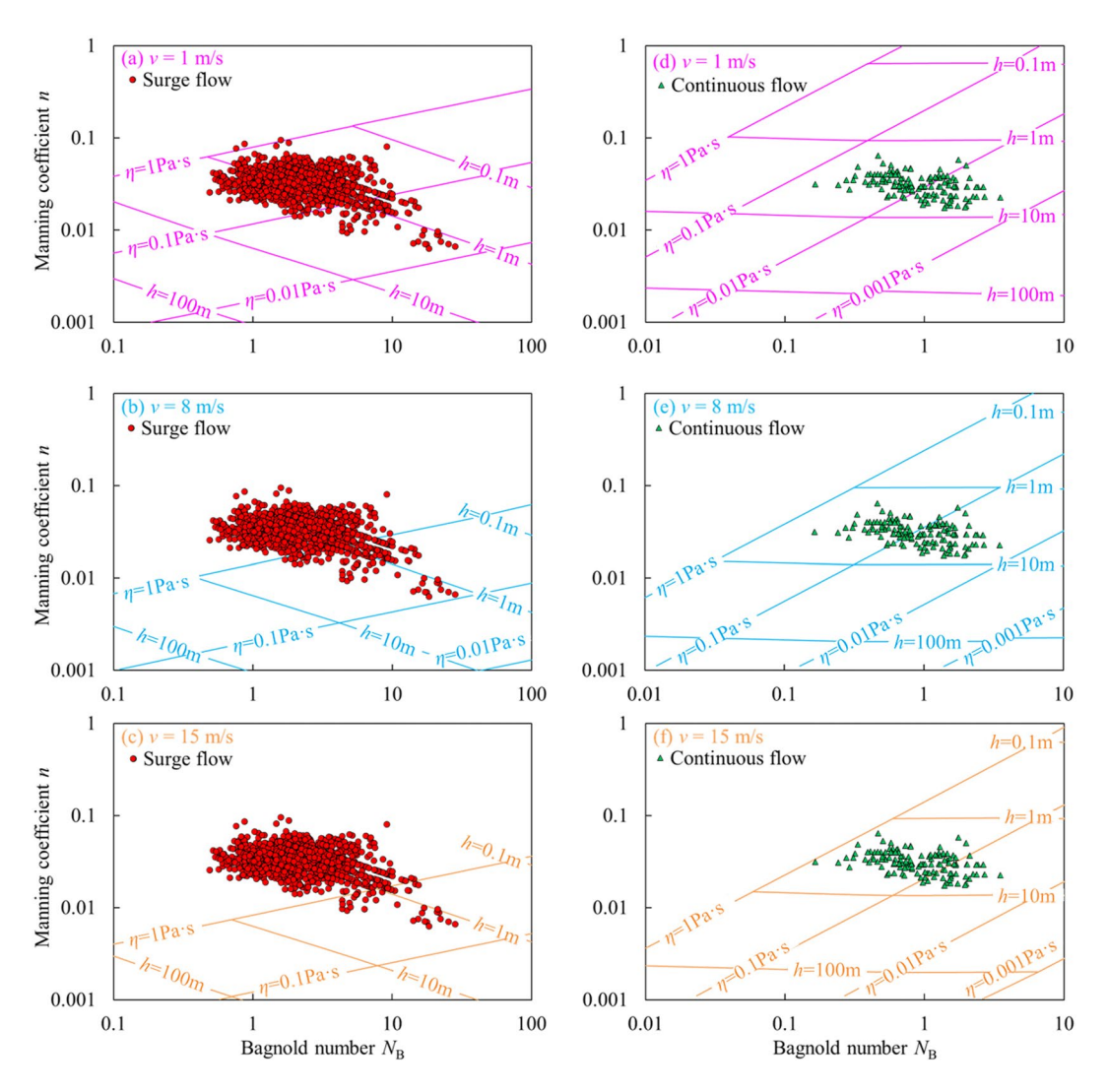


Figure 11. Comparison between field data and model prediction n-N_B relationship by Equation 15. For surge flow, (a–c) are the $(N_{\rm B}, n)$ theoretical planes with flow velocity v = 1, 8, and 15 m/s, respectively. For continuous flow, (d–f) are the $(N_{\rm B}, n)$ planes with flow velocity v = 1, 8, and 15 m/s, respectively.

(Figure 5) and relative viscosity (Figure 7). Given the idiosyncrasies of natural settings, the interpretation of field observations is often hindered by the discreteness resulting from the following three aspects. (a) The inclusion of large boulders (Imaizumi et al., 2016), particle-size segregation (Johnson et al., 2012), and complex boundary conditions (Iverson, 2003). (b) Ideal steady-state parameters are needed for analyzing the flow regime, which are easy to achieve in controlled experiments. However, the transient traits of natural debris flows indicate that the measurement is less accurate, especially, for the measurement of surge-flow height with splash (Wang et al., 2022) and the timing of flow fronts for determination of velocity (Nagl et al., 2020). (c) In addition, for the field observation data of debris flows, how to determine the critical particle size remains an open question. Its magnitude directly affects the accuracy of subsequent dynamic parameters, for example, the Stokes number (Figure 8b) and density ratio (Figure 8c).

The discreteness of field observation data is ubiquitous, but the debris flow dynamics behind the discreteness could still be revealed through appropriate statistics-based or physics-based (e.g., dimensionless groups) approaches. Based on the statistical analysis of a large number of field observation data, Rickenmann (1999) proposed the empirical relationships of debris flow, and these empirical relationships provided guiding significance for the mitigation of debris flow. Through the dynamic analysis of field observation data of Illgraben debris flows, the characteristics of the pore pressure response during movement (McArdell et al., 2007) and the erosion process of natural debris flows were revealed (Berger et al., 2011). Based on the field observation data of debris flows

CHEN ET AL. 16 of 22

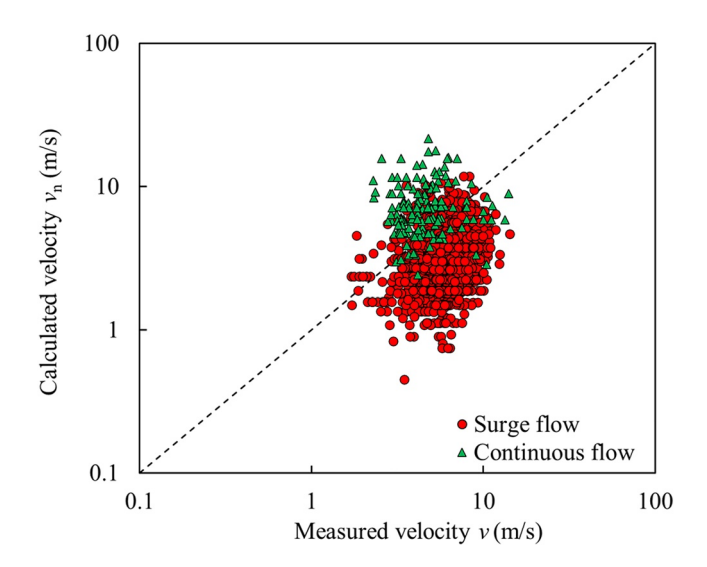


Figure 12. Comparison between the calculated velocities v_n and observed velocities v of Jiangjia Ravine debris flows.

in Chalk Cliffs (Colorado and Arroyo Seco, California), the power spectrum, and physics-based analysis showed that the periodic blockage-breaking effect is a significant reason for surge flows (Kean et al., 2013). Using field observation data of Jiangjia Ravine debris flows, probabilistic analysis showed that debris flow materials satisfy a universal grain size distribution, which strongly affects dynamic properties such as flow density, velocity, and discharge (Y. Li et al., 2014). Similarly, the discreteness of field observation data of Jiangjia Ravine debris flows cannot conceal the visco-collisional scaling law. Through physics-based analysis, the analysis of the flow regime shows a smooth transition from the fluid viscous effect to particle collisions, and the visco-collisional scaling law is further established.

5.2. The Visco-Collisional Scaling Law

The total solid concentration of Jiangjia Ravine debris flows could be as high as 0.85, and such high-density (up to 2,300 kg/m³) debris flows can move fast on a gentle slope ($\theta=3.7^{\circ}$), which prompts us to explore the source of flow resistance. With the transition from dense to dilute debris flows, the effective stress diminishes, and the flow gradually liquefies. In practical applications, flow resistance models (e.g., Equation 5) suitable for dense debris flows would be reduced to viscous fluid models. However, this study demonstrates

that the flow resistance not only comes from fluid viscosity but also from the visco-collisional effect jointly resisting the gravity that drives debris-flow movement.

Flow resistance can be well described by a visco-collisional scaling law (Equation 11). The flow-regime analysis shows that, regardless of surge or continuous flows, the flow regimes are distributed in both viscous and inertial regions (Figure 8a). However, for surge flows, the fitted constant b = 1.1 and is close to unity (note that this might be affected by the scattered field data). For continuous flows, the fitted constant b = 1.9. This indicates that the flow resistance of surge flows is mainly controlled by the viscous effect, while continuous flows mainly exhibit the characteristics of Bagnoldian flows (b = 2). Note that the viscous effect of surge flows is not exactly the same as the viscous drag of pure fluids, but a macroviscous regime of fluids containing a large number of particles (Bagnold, 1954; Davies, 1986). In other words, the macroscopic phenomena of surge and continuous flows can be quantitatively distinguished by the b value. For debris flows of other sites, macroscopic flow patterns (surge, continuous, and transitional flow) could also be quantitatively analyzed through this approach.

5.3. Phase Diagram of Natural Geophysical Flows

Solid concentration provides fundamental information concerning the mobility of debris flow. By comparing the rheologies of flows with different solid concentrations, a phase diagram can be summarized for natural debris flows (Figure 13). The overall trend of this phase diagram matches that of two-phase flows from the controlled laboratory experiments, which correlate the fluid viscosity with the change in solid concentration. However, for natural debris flows, the fluid viscosity is closely related to the fines (clay and silts) in the total solid content, which enriches the trends of viscous and collisional stresses in the phase diagram.

As shown in Figure 13, when the solid concentration is lower than 0.20 (McAnally et al., 2007), the sediment-laden flows are regarded as equivalent fluids. The flow regime is characterized by the relative viscosity of the equivalent fluid, η_s . The relative viscosity is solely a function of solid concentration, that is, $\eta_s(\varphi_s)$ (Krieger, 1972; Maron & Pierce, 1956). For flows dominated by the viscous effect, the flow resistance is rate-dependent and can be expressed as $\tau \sim \eta_s(\varphi_s)\eta\dot{\gamma}$.

As the solid concentration is higher than 0.60 (Major et al., 2005), the effective stress ($\sigma_e/\rho gh \cos \theta$) shows an increasing trend (pink line in Figure 13), so the contact friction ($\mu_p \sigma_e$) contributes to the flow resistance. In this regime, fluid viscosity, particle collisions, and friction coexist. The increase in contact friction results in weaker dependence of flow resistance on the shear rate but stronger dependence on normal stress. Flow resistance is described by the macroscopic friction coefficient μ and dimensionless parameter Π that characterizes the flow regime, that is, $\tau \sim \mu(\Pi)$. One example of the flow resistance models is the $\mu(K)$ law (Trulsson et al., 2012),

CHEN ET AL. 17 of 22

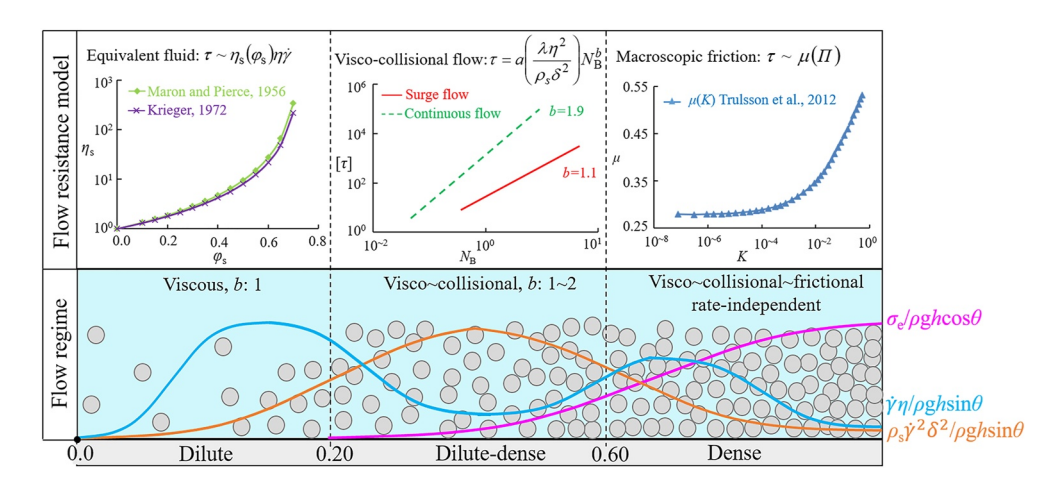


Figure 13. Phase diagram of geophysical flows, where fluid viscosity (fine content) increases with solid concentration. With the increase in solid concentration φ_s , the fluid regime undergoes viscous, visco-collisional, and visco-collisional-frictional dominance. Blue line, orange line, and pink line represent dimensionless viscous stress ($\dot{\gamma}\eta = \rho gh \sin \theta$), collisional stress ($\rho_s \dot{\gamma}^2 \delta^2 / \rho gh \sin \theta$), and effective stress ($\sigma_e / \rho gh \cos \theta$), respectively.

where K is a mixed dimensionless number, $K = J + \alpha I^2$, J is the viscous number, I is the inertial number, and α is a constant.

When the solid concentration is within the range (0.20, 0.60), debris flows transition from dilute to dense flow. The solid concentration of the Jiangjia Ravine debris flows is within this range. In this range, the flow resistance is not dominated by equivalent fluid viscosity, for example, the two viscosity laws of Krieger (1972) and Maron and Pierce (1956) for geophysical flows with lower solid concentrations, and the particle contact friction does not play a key role. For this transitional flow regime, the flow resistance is rate-dependent, b is between 1 and 2, and it can be well described by a visco-collisional scaling law (Equation 11), which bridges the gap between dilute and dense flows.

In Figure 13, viscous stress $(\dot{\gamma}\eta/\rho gh\sin\theta,$ blue line) shows double peaks, and collisional stress $(\rho_s\dot{\gamma}^2\delta^2/\rho gh\sin\theta,$ orange line) exhibits a single peak. When the solid concentration is lower than 0.20, with increasing solid concentration, the viscous stress and collisional stress both show increasing trends. However, the spacing between particles is much larger than the particle size, and the probability of particle collisions is low. Thus, the viscous effect dominates over particle collisions. At solid concentrations of 0.20–0.60, with increasing solid concentration and decreasing spacing between particles, collisional stress peaks. However, as the solid concentration approaches 0.6, the enhanced fluid viscosity by the fine content (clay and silts) enhances the viscous effect. When the solid concentration is higher than 0.60, the viscous stress and particle collisional stress decrease continuously, and particle contact friction starts to dominate.

In these above evolutions, the increasing viscous stress as the solid concentration approaches 0.6 marks the major difference between natural debris flows (Figure 13) and ideal two-phase flows in controlled experiments. For natural debris flows, the increase in fine content with increasing solid concentration enhances fluid viscosity. This cannot be observed in physical experiments because controlled experiments isolate the dependence of fluid viscosity on solid concentration (fine content).

In summary, in the series of flow regime evolutions, the particle interaction is gradually strengthened. Correspondingly, the flow resistance model is transformed from an equivalent fluid rheological framework ($\tau \sim \eta_s(\varphi_s)$) $\eta\dot{\gamma}$) to a visco-collisional scaling law ($\tau \sim a(N_B)^b$) and then to a friction law ($\tau \sim \mu(\Pi)$) where the shear stress is strongly related to the normal stress. More importantly, the fluid viscosity is closely related to the total solid concentration, thus the phase diagram of natural flows is distinct from that of the controlled experiments. The nontrivial evolution of the viscous effect and particle collisions in natural geophysical flows indicates that it is difficult to unify complex geophysical flows with a single flow resistance model.

CHEN ET AL. 18 of 22



5.4. The Modified Manning's Formula

Under fixed channel boundary conditions, by introducing physical mechanisms (visco-collisional effect) into the empirical description of flow resistance, the relationship between Manning's coefficient and flow regime (Bagnold number) is established. This relationship indicates that Manning's coefficient varies with the flow regime of debris flow. Therefore, compared with empirical Manning's coefficient, the modified Manning's coefficient $n(N_{\rm B})$ exhibits an explicit physical meaning, which is theoretically similar to the relationship between the drag coefficient and the Reynolds number. Therefore, for natural debris flows, the theoretical relationship between Manning's coefficient and flow regime should be universally applicable, although the parameters would be site specific.

The mobility of debris flow is an integral part of risk assessment (Kwan et al., 2021). In practice, Manning's coefficient is regarded as a constant in simulating the runout of geophysical flows (Delaney & Evans, 2015; Turzewski et al., 2019). However, based on the findings of this study, Manning's coefficient varies with the internal resistance associated with the flow regime. Thus, it is inappropriate to set Manning's coefficient as a constant to calculate the whole process of geophysical flow. In Equation 15, Manning's coefficient varies with flow depth and flow velocity. This can be improved by embedding this relationship in a numerical program.

6. Conclusions

For geophysical flows in natural settings, due to changes in solid concentration and fluid viscosity, distinct dynamic characteristics are exhibited. From dense debris flows to dilute debris flows, mobility demonstrates significant differences. Therefore, flow resistance has been the focus in the fields of geophysical science and fluid mechanics. Based on the field observation data of 93 debris-flow events at Jiangjia Ravine, this study explores the source of flow resistance from physical mechanisms and elaborates its potential application. The key conclusions are as follows:

- 1. For Jiangjia Ravine debris flows, the contribution of particle contact friction to flow resistance is negligible; rather, flow resistance comes from the particle collisional stress and the fluid viscous effect. The traditional equivalent fluid approach is invalid for debris flows with strong solid-fluid interactions.
- 2. Flow resistance can be well described by a visco-collisional scaling law. In this law, the exponent b reflects the properties of debris flow, and can be used as a feasible index for quantitatively distinguishing between surge flow and continuous flow. For the high-concentration surge flows, b is close to unity (b = 1.1), indicating that the viscous effect is more significant than the interaction of solid particles. This phenomenon is different from the general knowledge from controlled experiments where the effect of particles is dominant at higher solid concentrations. This is because the fluid viscosity increases with the fine content in high-concentration flows. For the low-concentration continuous flows, b is close to 2 (b = 1.9), indicating that the particle inertial collision dominates over the fluid viscous effect.
- 3. The flow resistance of the Jiangjia Ravine debris flow belongs to a rheological framework that strongly depends on the shear rate $(\tau \sim \dot{\gamma}^b)$. The visco-collisional scaling law is more conducive to explain the flow behavior than the pure-fluid rheological model. Thus, the governing equations considering the visco-collisional scaling law may yield more reasonable predictions for the dynamic evolution, mobility, and risk assessment of debris flow.
- 4. The theoretical relationship between Manning's coefficient and flow regime (as quantified by the Bagnold number) is established, where Manning's coefficient is assigned an explicit physical meaning and varies with the flow regime. Compared with the empirical Manning's coefficient, the modified Manning's coefficient provides a solid basis for the mobility and risk assessment of debris flow hazards.

Data Availability Statement

The field observation data of debris flows at Jiangjia Ravine from 1999 to 2017 were obtained from the Dongchuan Debris Flow Observation and Research Station (DDFORS), Chinese Academy of Sciences. All the field observation data used in this study are available at the National Cryosphere Desert Data Center via https://doi.org/10.12072/DDFORS.024.2019.db, https://doi.org/10.12072/ncdc.DDFORS.db0068.2020, https://doi.org/10.

CHEN ET AL. 19 of 22



12072/ncdc.DDFORS.db0066.2020, https://doi.org/10.12072/ncdc.DDFORS.db0037.2020, and https://doi.org/10.12072/ncdc.ddfors.db2689.2023 with registrations (Hong, 2016, 2019a, 2019b, 2019c; Li & Hong, 2022).

Acknowledgments

This study is supported by the National Natural Science Foundation of China (41925030 and 42077256). We would like to thank the Dongchuan Debris Flow Observation and Research Station (DDFORS), Chinese Academy of Sciences, which provides the field observation data of Jiangjia Ravine debris flows.

References

- Ancey, C. (2007). Plasticity and geophysical flows: A review. Journal of Non-Newtonian Fluid Mechanics, 142(1), 4–35. https://doi.org/10.1016/j.innfm.2006.05.005
- Ancey, C., & Evesque, P. (2000). Frictional-collisional regime for granular suspension flows down an inclined channel. *Physical Review E*, 62(6), 8349–8360. https://doi.org/10.1103/PhysRevE.62.8349
- Bagnold, R. A. (1954). Experiments on a gravity-free dispersion of large solid spheres in a Newtonian fluid under shear. *Proceedings of the Royal Society of London Series A*, 225, 49. https://doi.org/10.1098/rspa.1954.0186
- Bartelt, P., Bühler, Y., Buser, O., Christen, M., & Meier, L. (2012). Modeling mass-dependent flow regime transitions to predict the stopping and depositional behavior of snow avalanches. *Journal of Geophysical Research*, 117(F1). https://doi.org/10.1029/2010JF001957
- Batchelor, G., & Green, J. (1972). The determination of the bulk stress in a suspension of spherical particles to order c2. *Journal of Fluid Mechanics*, 56(3), 401–427. https://doi.org/10.1017/S0022112072002435
- Bellos, V., Nalbantis, I., & Tsakiris, G. (2018). Friction modeling of flood flow simulations. *Journal of Hydraulic Engineering*, 144(12), 04018073. https://doi.org/10.1061/(asce)hy.1943-7900.0001540
- Berger, C., McArdell, B. W., & Schlunegger, F. (2011). Direct measurement of channel erosion by debris flows, Illgraben, Switzerland. *Journal of Geophysical Research*, 116(F1), F01002. https://doi.org/10.1029/2010JF001722
- Berzi, D., & Larcan, E. (2013). Flow resistance of inertial debris flows. *Journal of Hydraulic Engineering*, 139(2), 187–194. https://doi.org/10.1061//ASCE/HY.1943-7900.0000664
- Boyer, F., Guazzelli, E., & Pouliquen, O. (2011). Unifying suspension and granular rheology. *Physical Review Letters*, 107(18), 188301. https://doi.org/10.1103/PhysRevLett.107.188301
- Cao, Z., Li, J., Pender, G., & Liu, Q. (2015). Whole-process modeling of reservoir turbidity currents by a double layer-averaged model. *Journal of Hydraulic Engineering*, 141(2), 04014069. https://doi.org/10.1061/(ASCE)HY.1943-7900.0000951
- Cassar, C., Nicolas, M., & Pouliquen, O. (2005). Submarine granular flows down inclined planes. *Physics of Fluids*, 17(10), 103301. https://
- doi.org/10.1063/1.2069864

 Courrech du Pont, S., Gondret, P., Perrin, B., & Rabaud, M. (2003). Granular avalanches in fluids. *Physical Review Letters*, 90(4), 044301. htt
- ps://doi.org/10.1103/PhysRevLett.90.044301 Coussot, P. (1995). Structural similarity and transition from Newtonian to non-Newtonian behavior for clay-water suspensions. *Physical Review*
- Letters, 74(20), 3971–3974. https://doi.org/10.1103/PhysRevLett.74.3971
 Cui, P., Chen, X., Waqng, Y., Hu, K., & Li, Y. (2005). Jiangjia Ravine debris flows in south-western China. In P. Cui, X. Chen, Y. Waqng, K. Hu,
- & Y. Li (Eds.), Debris-flow hazards and related phenomena (pp. 565–594). Springer. https://doi.org/10.1007/3-540-27129-5_22

 Cui, P., Tang, J., & Lin, P. (2016). Research progress of resistance character of debris-flow. Journal of Si Chuan University (Engineering Science
- Edition), 48(03), 1–11. (in Chinese). https://doi.org/10.15961/j.jsuese.2016.03.001

 Davies, T. R. H. (1986). Large debris flows: A macro-viscous phenomenon. Acta Mechanica, 63(1–4), 161–178. https://doi.org/10.1007/BF01
- 182546
 Davies, T. R. H. (1990). Debris-flow surges Experimental simulation. *Journal of Hydrology*, 29(1), 18–46. Retrieved from https://www.js
- tor.org/stable/43944650
- Delaney, K. B., & Evans, S. G. (2015). The 2000 Yigong landslide (Tibetan Plateau), rockslide-dammed lake and outburst flood: Review, remote sensing analysis, and process modelling. *Geomorphology*, 246, 377–393. https://doi.org/10.1016/j.geomorph.2015.06.020
- Du, C., Wu, W., & Ma, C. (2021). Velocity profile of debris flow based on quadratic rheology model. *Journal of Mountain Science*, 18(8), 2120–2129. https://doi.org/10.1007/s11629-021-6790-7
- Egashira, S. (2011). Prospects of debris flow studies from constitutive relations to governing equations. *Journal of Disaster Research*, 6(3), 313–320. https://doi.org/10.20965/jdr.2011.p0313
- Einstein, A. (1905). Eine neue bestimmung der moleküldimensionen. ETH Zurich.
- Fei, X. J., Kang, Z. C., & Wang, Y. Y. (1991). Effect of the fine grain and debris flow slurry bodies on debris flow motion. *Mountain Research*, 9(3), 143–152. (in Chinese). Retrieved from http://shandixb.paperonce.org/oa/DArticle.aspx?type=view&id=199126
- Ferguson, R. (2005). Estimating critical stream power for bedload transport calculations in gravel-bed rivers. *Geomorphology*, 70(1–2), 33–41. https://doi.org/10.1016/j.geomorph.2005.03.009
- Guo, X. J., Li, Y., Cui, P., Yan, H., & Zhuang, J. (2020). Intermittent viscous debris flow formation in Jiangjia Gully from the perspectives of hydrological processes and material supply. *Journal of Hydrology*, 589, 125184. https://doi.org/10.1016/j.jhydrol.2020.125184
- Hong, Y. (2016). Movement elements and general observation statistics of debris flow in Jiangjia gully, Dongchuan, Yunnan, 1999-2005 [Dataset]. National Cryosphere Desert Data Center. https://doi.org/10.12072/DDFORS.024.2019.db
- Hong, Y. (2019a). Movement factors and overall observation statistics of debris flow in Jiangjiagou, Dongchuan, Yunnan in 2013 [Dataset]. National Cryosphere Desert Data Center. https://doi.org/10.12072/ncdc.DDFORS.db0068.2020
- Hong, Y. (2019b). Movement factors and overall observation statistics of debris flow in Jiangjiagou, Dongchuan, Yunnan in 2014 [Dataset]. National Cryosphere Desert Data Center. https://doi.org/10.12072/ncdc.DDFORS.db0066.2020
- Hong, Y. (2019c). Movement factors and overall observation statistics of debris flow in Jiangjiagou, Dongchuan, Yunnan in 2017 [Dataset]. National Cryosphere Desert Data Center. https://doi.org/10.12072/ncdc.DDFORS.db0037.2020
- Hsu, L., Dietrich, W. E., & Sklar, L. S. (2014). Mean and fluctuating basal forces generated by granular flows: Laboratory observations in a large vertically rotating drum. *Journal of Geophysical Research: Earth Surface*, 119(6), 1283–1309. https://doi.org/10.1002/2013jf003078
- Hungr, O. (1995). A model for the runout analysis of rapid flow slides, debris flows, and avalanches. Canadian Geotechnical Journal, 32(4), 610–623. https://doi.org/10.1139/t95-063
- Hungr, O., & McDougall, S. (2009). Two numerical models for landslide dynamic analysis. Computers and Geosciences, 35(5), 978–992. https://doi.org/10.1016/j.cageo.2007.12.003
- Huthoff, F. (2012). Theory for flow resistance caused by submerged roughness elements. *Journal of Hydraulic Research*, 50(1), 10–17. https://doi.org/10.1080/00221686.2011.636635
- Huybrechts, N., Vu Luong, G., Zhang, Y., & Verbanck, M. A. (2011). Observations of canonical flow resistance in fast-flowing sand bed rivers. Journal of Hydraulic Research, 49(5), 611–616. https://doi.org/10.1080/00221686.2011.596651

CHEN ET AL. 20 of 22

0001-8686(72)80001-0



- Imaizumi, F., Tsuchiya, S., & Ohsaka, O. (2016). Behavior of boulders within a debris flow initiation zone. *International Journal of Erosion Control Engineering*, 9(3), 91–100. https://doi.org/10.13101/ijece.9.91
- Iverson, R. M. (1997). The physics of debris flows. Reviews of Geophysics, 35(3), 245-296. https://doi.org/10.1029/97RG00426
- Iverson, R. M. (2000). Landslide triggering by rain infiltration. Water Resources Research, 36(7), 1897–1910. https://doi.org/10.1029/2000WR
- Iverson, R. M. (2003). How should mathematical models of geomorphic processes be judged? In *Prediction in geomorphology*, (pp. 83–94). https://doi.org/10.1029/135GM07
- Iverson, R. M. (2005). Regulation of landslide motion by dilatancy and pore pressure feedback. *Journal of Geophysical Research*, 110(F2), F02015. https://doi.org/10.1029/2004JF000268
- Iverson, R. M., & George, D. L. (2014). A depth-averaged debris-flow model that includes the effects of evolving dilatancy. I. Physical basis. Proceedings of the Royal Society A: Mathematical, Physical & Engineering Sciences, 470(2170), 20130819. https://doi.org/10.1098/rspa. 2013.0819
- Johnson, C. G., Kokelaar, B. P., Iverson, R. M., Logan, M., LaHusen, R. G., & Gray, J. M. N. T. (2012). Grain-size segregation and levee formation in geophysical mass flows. *Journal of Geophysical Research*, 117(F1), F01032. https://doi.org/10.1029/2011JF002185
- Julien, P. Y., & Paris, A. (2010). Mean velocity of mudflows and debris flows. Journal of Hydraulic Engineering, 136(9), 676–679. https://doi.org/10.1061/(ASCE)HY.1943-7900.0000224
- Kaitna, R., Palucis, M. C., Yohannes, B., Hill, K. M., & Dietrich, W. E. (2016). Effects of coarse grain size distribution and fine particle content on pore fluid pressure and shear behavior in experimental debris flows. *Journal of Geophysical Research: Earth Surface*, 121(2), 415–441. https://doi.org/10.1002/2015jf003725
- Kang, Z. C., Lee, C. F., Ma, A. N., & Luo, J. T. (2004). Research on debris flow in China (pp. 213–224). Science Press. Retrieved from https://192.168.143.20:8080/handle/131551/3663
- Kean, J. W., McCoy, S. W., Tucker, G. E., Staley, D. M., & Coe, J. A. (2013). Runoff-generated debris flows: Observations and modeling of surge initiation, magnitude, and frequency. *Journal of Geophysical Research: Earth Surface*, 118(4), 2190–2207. https://doi.org/10.1002/jgrf.20148
 Krieger, I. M. (1972). Rheology of monodisperse latices. *Advances in Colloid and Interface Science*, 3(2), 111–136. https://doi.org/10.1016/
- Kwan, J. S. H., Sze, E. H. Y., Lam, C., Law, R. P. H., & Koo, R. C. H. (2021). Development and applications of debris mobility models in Hong Kong. Proceedings of the Institution of Civil Engineers Geotechnical Engineering, 174(5), 593–610. https://doi.org/10.1680/jgeen.21.00008
- Lanzoni, S., Gregoretti, C., & Stancanelli, L. M. (2017). Coarse-grained debris flow dynamics on erodible beds. *Journal of Geophysical Research:* Earth Surface, 122(3), 592–614. https://doi.org/10.1002/2016JF004046
- Li, J., Cao, Z., Hu, K., Pender, G., & Liu, Q. (2018). A depth-averaged two-phase model for debris flows over erodible beds. Earth Surface Processes and Landforms. 43(4), 817–839, https://doi.org/10.1002/esp.4283
- Li, X. Y., & Hong, Y. (2022). Observation data of debris flow in Jiangjiagou, Dongchuan, Yunnan, 2006–2010 [Dataset]. National Cryosphere Desert Data Center. https://doi.org/10.12072/ncdc.ddfors.db2689.2023
- Li, Y., Liu, J., Su, F., Xie, J., & Wang, B. (2014). Relationship between grain composition and debris flow characteristics: A case study of the Jiangjia Gully in China. Landslides, 12(1), 19–28. https://doi.org/10.1007/s10346-014-0475-z
- Major, J. J., Pierson, T. C., Scott, K. M., Jakob, M., & Hungr, O. (2005). Debris flows at mount St. Helens, Washington, USA. In M. Jakob & O. Hungr (Eds.), *Debris-flow hazards and related phenomena* (pp. 685–731). Springer Berlin Heidelberg. https://doi.org/10.1007/3-540-27129-5_27
- Maron, S. H., & Pierce, P. E. (1956). Application of ree-eyring generalized flow theory to suspensions of spherical particles. *Journal of Colloid Science*, 11(1), 80–95. https://doi.org/10.1016/0095-8522(56)90023-X
- McAnally, W. H., Friedrichs, C., Hamilton, D., Hayter, E., Shrestha, P., Rodriguez, H., et al. (2007). Management of fluid mud in estuaries, Bays, and lakes. I: Present state of understanding on character and behavior. *Journal of Hydraulic Engineering*, 133(1), 9–22. https://doi.org/10.1061/(ASCE)0733-9429(2007)133:1(9)
- McArdell, B. W., Bartelt, P., & Kowalski, J. (2007). Field observations of basal forces and fluid pore pressure in a debris flow. *Geophysical Research Letters*, 34(7), L07406. https://doi.org/10.1029/2006GL029183
- McDougall, S., & Hungr, O. (2004). A model for the analysis of rapid landslide motion across three-dimensional terrain. *Canadian Geotechnical Journal*, 41(6), 1084–1097. https://doi.org/10.1139/t04-052
- Naef, D., Rickenmann, D., Rutschmann, P., & McArdell, B. W. (2006). Comparison of flow resistance relations for debris flows using a one-dimensional finite element simulation model. *Natural Hazards and Earth System Sciences*, 6(1), 155–165. https://doi.org/10.5194/nhess-6-155-2006
- Nagl, G., Hübl, J., & Kaitna, R. (2020). Velocity profiles and basal stresses in natural debris flows. Earth Surface Processes and Landforms, 45(8), 1764–1776. https://doi.org/10.1002/esp.4844
- Nikora, V. I., Goring, D. G., & Biggs, B. J. (1998). On gravel-bed roughness characterization. Water Resources Research, 34(3), 517–527. https://doi.org/10.1029/97WR02886
- O'Brien, J. S., Julien, P. Y., & Fullerton, W. T. (1993). Two-Dimensional water flood and mudflow simulation. *Journal of Hydraulic Engineering*, 119(2), 244–261. https://doi.org/10.1061/(ASCE)0733-9429(1993)119:2(244)
- Ouyang, C., He, S., Xu, Q., Luo, Y., & Zhang, W. (2013). A MacCormack-TVD finite difference method to simulate the mass flow in mountainous terrain with variable computational domain. *Computers and Geosciences*, 52, 1–10. https://doi.org/10.1016/j.cageo.2012.08.024
- Özgen, I., Teuber, K., Simons, F., Liang, D., & Hinkelmann, R. (2015). Upscaling the shallow water model with a novel roughness formulation. Environmental Earth Sciences, 74(11), 7371–7386. https://doi.org/10.1007/s12665-015-4726-7
- Pailha, M., & Pouliquen, O. (2009). A two-phase flow description of the initiation of underwater granular avalanches. *Journal of Fluid Mechanics*, 633, 115–135. https://doi.org/10.1017/S0022112009007460
- Pierson, T. C. (1981). Dominant particle support mechanisms in debris flows at Mt Thomas, New Zealand, and implications for flow mobility. Sedimentology, 28(1), 49–60. https://doi.org/10.1111/j.1365-3091.1981.tb01662.x
- Pudasaini, S. P. (2012). A general two-phase debris flow model. Journal of Geophysical Research, 117(F3), F03010. https://doi.org/10.1029/ 2011JF002186
- Pudasaini, S. P., & Mergili, M. (2019). A multi-phase mass flow model. Journal of Geophysical Research: Earth Surface, 124(12), 2920–2942. https://doi.org/10.1029/2019JF005204
- Rauter, M., Fischer, J. T., Fellin, W., & Kofler, A. (2016). Snow avalanche friction relation based on extended kinetic theory. Natural Hazards and Earth System Sciences, 16(11), 2325–2345. https://doi.org/10.5194/nhess-16-2325-2016
- Rickenmann, D.~(1999).~Empirical~relationships~for~debris~flows.~Natural~Hazards,~19(1),~47-77.~https://doi.org/10.1023/A:1008064220727.
- Sairam, N., Brill, F., Sieg, T., Farrag, M., Kellermann, P., Nguyen, V. D., et al. (2021). Process-based flood risk assessment for Germany. Earth's Future, 9(10), e2021EF002259. https://doi.org/10.1029/2021EF002259

CHEN ET AL. 21 of 22



- Song, D., Zhou, G. G. D., & Chen, Q. (2021). Flow resistance in the transition from dense to dilute granular-fluid flows. *Granular Matter*, 23(3), 73. https://doi.org/10.1007/s10035-021-01134-1
- Sosio, R., & Crosta, G. B. (2009). Rheology of concentrated granular suspensions and possible implications for debris flow modeling. *Water Resources Research*, 45(3), W03412. https://doi.org/10.1029/2008WR006920
- Sosio, R., Crosta, G. B., & Frattini, P. (2007). Field observations, rheological testing and numerical modelling of a debris-flow event. Earth Surface Processes and Landforms, 32(2), 290–306. https://doi.org/10.1002/esp.1391
- Stewart, M. T., Cameron, S. M., Nikora, V. I., Zampiron, A., & Marusic, I. (2019). Hydraulic resistance in open-channel flows over self-affine rough beds. *Journal of Hydraulic Research*, 57(2), 183–196. https://doi.org/10.1080/00221686.2018.1473296
- Stickel, J. J., & Powell, R. L. (2005). Fluid mechanics and rheology of dense suspensions. *Annual Review of Fluid Mechanics*, 37(1), 129–149. https://doi.org/10.1146/annurev.fluid.36.050802.122132
- Trulsson, M., Andreotti, B., & Claudin, P. (2012). Transition from the viscous to inertial regime in dense suspensions. *Physical Review Letters*, 109(11), 118305. https://doi.org/10.1103/PhysRevLett.109.118305
- Turzewski, M. D., Huntington, K. W., & LeVeque, R. J. (2019). The geomorphic impact of outburst floods: Integrating observations and numerical simulations of the 2000 Yigong flood, Eastern Himalaya. *Journal of Geophysical Research: Earth Surface*, 124(5), 1056–1079. https://doi.org/10.1029/2018JF004778
- Wang, L., Song, D., Zhou, G. G. D., Chen, X. Q., Xu, M., Choi, C. E., & Peng, P. (2022). Debris flow overflowing flexible barrier: Physical process and drag load characteristics. *Landslides*, 19(8), 1881–1896. https://doi.org/10.1007/s10346-022-01880-0
- Wildemuth, C., & Williams, M. (1984). Viscosity of suspensions modeled with a shear-dependent maximum packing fraction. *Rheologica Acta*, 23(6), 627–635. https://doi.org/10.1007/BF01438803
- Yang, H., Wei, F. Q., & Hu, K. H. (2012). Contrast tests for models on viscous debris flow using observations from Jiangjiagou watershed. *Bulletin of Soil and Water Conservation*, 32(03), 182–187. (in Chinese). https://doi.org/10.13961/j.cnki.stbctb.2012.03.010
- Yen, B. C. (1992). Dimensionally homogeneous Manning's formula. *Journal of Hydraulic Engineering*, 118(9), 1326–1332. https://doi.org/10.1061/(ASCE)0733-9429(1992)118:9(1326)
- Zhou, G. G. D., & Ng, C. W. (2010). Dimensional analysis of natural debris flows. Canadian Geotechnical Journal, 47(7), 719–729. https://doi.org/10.1139/t09-134